



Fermi National Accelerator Laboratory

FERMILAB Pub-94/123

## Charmonium Formation in $p\bar{p}$ Annihilations

R. Cester

*I.N.F.N. and Department of Experimental Physics, University of Turin  
via Pietro Giuria 1, 10125 Torino, Italy*

P.A. Rapidis

*Fermi National Accelerator Laboratory  
P.O. Box 500, Batavia, Illinois 60510*

May 1994

To appear in *Annual Review of Nuclear and Particle Science*



## **Disclaimer**

*This report was prepared as an account of work sponsored by an agency of the United States Government. Neither the United States Government nor any agency thereof, nor any of their employees, makes any warranty, express or implied, or assumes any legal liability or responsibility for the accuracy, completeness, or usefulness of any information, apparatus, product, or process disclosed, or represents that its use would not infringe privately owned rights. Reference herein to any specific commercial product, process, or service by trade name, trademark, manufacturer, or otherwise, does not necessarily constitute or imply its endorsement, recommendation, or favoring by the United States Government or any agency thereof. The views and opinions of authors expressed herein do not necessarily state or reflect those of the United States Government or any agency thereof.*

# CHARMONIUM FORMATION IN $p\bar{p}$ ANNIHILATIONS

R. Cester

I.N.F.N. and Department of Experimental Physics, University of Turin,  
via Pietro Giuria 1, 10125 Torino, Italy

P. A. Rapidis

Fermilab\*, P.O. Box 500, Batavia, Illinois 60510

## CONTENTS

1. INTRODUCTION .....	2
2. THE ANNIHILATION SOURCE .....	5
2.1 The Beam .....	5
2.2 The Target .....	7
2.3 Beam Energy Measurements .....	8
2.4 The Fermilab Annihilation Source .....	9
3. EXPERIMENTAL TECHNIQUE .....	12
3.1 Analysis of a Resonance Excitation Curve .....	12
3.2 Event Detection and Analysis .....	14
3.3 Luminosity Measurement .....	16
3.4 Determination of the Energy Spectrum .....	16
4. EXPERIMENTAL RESULTS .....	17
4.1 The $J/\psi$ and the $\psi'$ .....	17
4.2 An aside: the Proton Electromagnetic Form Factor .....	19
4.3 The $1^3P_J$ Triplet .....	21
4.4 The 'Missing' $1^1P_1$ .....	24
4.5 The $p\bar{p} \rightarrow (c\bar{c}) \rightarrow \gamma\gamma$ Process .....	26

---

\* Operated by the Universities Research Association under contract no. DE-AC02-76CHO3000 with the U.S. Department of Energy.

5 INTERPRETATION OF THE EXPERIMENTAL RESULTS .....	30
5.1 Charmonium Dynamics .....	30
5.2 Charmonium Decay Rates .....	32
5.3 Determination of $\alpha_S$ from Charmonium Data .....	35
6. OUTLOOK .....	37

## 1 INTRODUCTION

The experimental study of high-momentum-transfer lepton scattering by nucleons in the late 1960's demonstrated that to these probes nucleons appear as structures of nearly free elementary constituents (partons). The interpretation of these experiments brought forward the hypothesis that the strength of hadronic interactions could change with energy from the low energy regime of 'infrared slavery' where constituents are inescapably bound within the hadron, to a high energy regime of 'asymptotic freedom', where the interaction between constituents becomes progressively weaker. Soon after it was shown [1] that a class of renormalizable field theories, invariant under the transformations of a non-abelian gauge group, exhibit this ultra-violet asymptotic behaviour. To this class of theories belongs Quantum Chromodynamics(QCD). This theory, based on the color  $SU_3$  gauge group, describes the phenomenology of hadron dynamics well, and is at present considered to be a viable theory of strong interactions.

The discovery[2] of the  $J/\psi$  and  $\psi'$  states of charmonium in the fall of 1974 was, in this context, of crucial importance. The observation of these positronium-like bound states of a heavy quark-antiquark pair ( $\bar{c}c$ ) provided the important experimental observation required to establish the credibility of the then nascent idea of asymptotic freedom in quantum chromodynamics. Furthermore, the subsequent observation of a coulomb-like spectrum of charmonium states[3] established "... charmonium as the 'hydrogen atom' of strong interaction physics. For it then became possible to subject the gauge theories of strong interactions to fairly stringent tests in a reasonably simple setting. Much of hadronic physics could then be related to charmonium spectroscopy as molecular spectra are related to that of hydrogen"[4]. These early words have indeed turned out to be almost prophetic: a veritable flood

of charmonium inspired theoretical investigations and phenomenology[5], as well as lattice gauge calculations[6] has appeared in the physics literature since then.

The earlier studies of charmonium states and their decays were carried out almost exclusively at  $e^+e^-$  colliders. In such experiments the electron-positron annihilation proceeds primarily through an intermediate virtual photon to the creation of a bound quark-antiquark charmonium state. This production mechanism limits the quantum numbers of the final states to be those of the photon, i.e.,  $J^{PC} = 1^{--}$ . Thus the orthocharmonium states  $J/\psi[1^3S_1]$ , and  $\psi'[2^3S_1]$ , as well as the  $\psi(3770)[1^3D_1]$  state<sup>1</sup>, are readily produced in  $e^+e^-$  collisions, where they appear as narrow resonances. The major advantage of studying in  $e^+e^-$  collisions the formation of charmonium resonances, which then decay to a hadronic final state, is the high yield, much higher than the rate for the underlying hadronic continuum. The peak ratio for these two processes is  $\sim 300$  at the  $J/\psi$  and  $\sim 120$  at the  $\psi'$ . For these states, precise measurements of their mass and width can be obtained from the energy of the electron and positron beams which are accurately known.

States such as the paracharmonium  $\eta_c[1^1S_0]$  and  $\eta'_c[2^1S_0]$ , or the orbitally excited states  $\chi_{c0}[1^3P_0]$ ,  $\chi_{c1}[1^3P_1]$ ,  $\chi_{c2}[1^3P_2]$ , and  $h_c[1^1P_1]$ , cannot be directly produced in  $e^+e^-$  collisions. All of these states have been studied in  $e^+e^-$  collisions through the cascade decays of the  $\psi$ 's (e.g.,  $\psi' \rightarrow \gamma\chi_{c2} \rightarrow \gamma\gamma J/\psi$ , or  $J/\psi \rightarrow \gamma\eta_c \rightarrow \gamma K\bar{K}\pi$ ). In these cases the precision of the measurement of their properties has been limited by the resolution of the detection equipment. In addition, states for which the cascade from the  $\psi'$  involves unfavorable branching ratios or multiple steps (e.g.,  $\psi' \rightarrow \gamma\eta'_c$ , and even worse  $\psi' \rightarrow \gamma\eta'_c \rightarrow \gamma\gamma h_c$ ) have remained unobserved or poorly studied.

An alternative way to study charmonium is through proton-antiproton annihilation. This process differs from the electron-positron annihilation in two important ways: first, the composite nature of the proton (and of the antiproton) allows the direct formation of all charmonium states, i.e., one is not limited to  $J^{PC} = 1^{--}$  states; second, the combination of a large non-resonant cross section for the process  $p\bar{p} \rightarrow \text{hadrons}$  ( $\sim 70$  mbarn) and of

---

<sup>1</sup>We use the usual spectroscopic notation  $n^{(2S+1)}L_J$ , where  $n$  is the principal quantum number, which is equal to one plus the number of nodes in the radial wave function, and  $L, S$ , and  $J$  are the orbital, spin, and total angular momentum of the quark-antiquark system. For a fermion-antifermion system the parity is given by  $P = (-)^{(L+1)}$ , and the charge conjugation parity by  $C = (-)^{(L+S)}$ .

the rather small cross sections for  $p\bar{p} \rightarrow (c\bar{c})$  ( $\sim 1 \mu\text{barn}$  at best), leads to an unfavorable signal to noise ratio. Thus, even though the suggestion of using this alternative method was proposed quite early[7], the fruition of this idea had to await a significant technological advance: the advent of stochastic cooling.

Stochastic cooling[8] is a technique used to decrease the phase space of dilute beams and obtain dense beams. It was the significant step in the program that led to the successful operation of high energy proton-antiproton colliders[9]. A direct spin-off of that program was the availability of dense beams of stochastically cooled  $\bar{p}$ 's with precisely controlled momentum and extremely narrow momentum spread ( $dp/p \sim .01\%$ ). In 1979 it was realized[10] that such a beam impinging on a stationary hydrogen target, with the appropriate energy to form a charmonium resonance, provided all the ingredients for a successful experiment. The precisely defined momentum and the narrow momentum spread of the antiproton beam allowed for excellent resolution in the *initial* state, which in turn allowed for a precise and direct measurement of the mass and width of a charmonium resonance. Furthermore, it was recognized that by selecting charmonium decays into electromagnetic final states with either a high mass  $e^+e^-$  pair or a high mass pair of  $\gamma$ 's, one could observe a signal even in the presence of a ferocious non-resonant hadronic background.

Two experiments to date have studied charmonium production in  $p\bar{p}$  annihilation, R704 at CERN[11] and E760 at Fermilab[12]. Both experiments incorporate the features outlined in Ref.[10]. A continuously stochastically cooled beam of antiprotons of variable, but well controlled momentum and of a small momentum spread circulates in a storage ring. The target used is a molecular-cluster hydrogen gas jet perpendicular to the beam. The stochastic cooling system preserves the beam's emittance and counteracts the small energy loss inside the target providing a beam with constant energy, small energy spread and long lifetime. This leads to an optimal utilization of the antiprotons, which are very costly to produce.

The excitation curve for a charmonium resonance is obtained as a function of the center-of-mass energy for processes such as :

$$p\bar{p} \rightarrow (c\bar{c}) \rightarrow e^+e^- \quad (1)$$

$$p\bar{p} \rightarrow (c\bar{c}) \rightarrow J/\psi X \rightarrow e^+e^- X \quad (2)$$

$$p\bar{p} \rightarrow (c\bar{c}) \rightarrow \gamma\gamma, \quad (3)$$

where  $(c\bar{c})$  is a charmonium resonance decaying into the indicated final state (if such a decay is allowed). These final states can be efficiently identified, in the presence of the large non-resonant background, by using a detection apparatus that includes a large-acceptance electromagnetic calorimeter and Cherenkov counter. The combination of these two detection techniques, together with charged particle hodoscopes and tracking, allows the rejection of hadrons. In addition, the implementation of a two-arm trigger logic that accepts events with  $e^+e^-$  or  $\gamma\gamma$  that are almost back-to-back in the center of mass (a characteristic of a decay of a high mass state) further reduces the background. From the study of the excitation curve one determines the mass ( $M_R$ ), total width ( $\Gamma_{tot}$ ), and the product of the branching ratios  $B_{p\bar{p}}B_f$  of the charmonium state under study into the initial ( $B_{p\bar{p}} = \Gamma_{p\bar{p}}/\Gamma_{tot}$ ) and final states (e.g., for a  $\gamma\gamma$  final state  $B_f \equiv B_{\gamma\gamma} = \Gamma_{\gamma\gamma}/\Gamma_{tot}$ ). Given the excellent resolution in the center-of-mass energy, one can measure directly the total width of even the  $J/\psi$ , the narrowest charmonium state.

## 2 THE ANNIHILATION SOURCE

The characteristics of the annihilation source (instantaneous luminosity, energy definition and control, source dimensions etc.) determine the quality of an experiment of this type. In this section we will first describe in some detail the R704 setup [2.1 to 2.3] to emphasize the novelty of the approach. In section 2.4 we will summarize the distinctive features of E760 that led to an improvement in source performance over R704.

### 2.1 The Beam

In a formation experiment, where antiprotons interact on a stationary hydrogen target, the energy of the beam is related to the value of the mass of the resonance by the equation:

$$E_{\bar{p}} = \frac{M_R^2}{2m_p} - m_p \quad (4)$$

with  $m_p$  the mass of the proton. To study the formation of charmonium states in the mass range  $2950 \leq M_R \leq 3850$  MeV/ $c^2$  one needs a beam of

momentum ranging from 3.6 to 6.9 GeV/c.

When R704 was proposed there was no antiproton storage ring operating in this momentum range. It was suggested that, with some modifications, it would be possible to utilize for such an experiment one of the rings of the CERN Intersecting Storage Rings (ISR)[13]. When the ISR were operated as a  $\bar{p}p$  collider, particles of opposite charge were transferred to the two ISR rings after having been accelerated in the Proton Synchrotron (PS) to a momentum of 26 GeV/c. For R704, on the other hand, the 3.5 GeV/c beam from the Antiproton Accumulator (AA) was transferred to ring 2 of the ISR without acceleration in the PS which now acted simply as a segment of the transfer line. To increase the transfer efficiency the large emittance antiproton beam from the AA was extracted in three successive slices then recombined in a single pulse by the ISR momentum cooling system. The maximum number of antiprotons stored for R704 was  $N_{\bar{p}} = 1.1 \times 10^{11}$ .

The ISR RF system was not sufficiently powerful to capture the low energy beam and shortly after injection the beam lost its bunched structure. The antiprotons were then brought to the chosen energy by phase displacement acceleration, a method applicable to unbunched beams[14]. Because the beam emittance deteriorated significantly during acceleration, further cooling was necessary before data taking could begin.

Transverse betatron cooling and momentum cooling were available in ring 2 of the ISR for high energy operation and were easily adapted to low energy operation by adding variable delay lines to each system. Vertical betatron cooling was used in this experiment to combat the vertical blow-up of the antiproton beam, caused by multiple scattering in the traversals of the target. The momentum cooling system was essential to the experiment: it reduced the spread of the beam momentum after injection and after acceleration; it compensated for the energy loss in the target ( $\sim 20$  MeV/day), thus holding the beam momentum constant during data taking. The momentum cooling system also served as a horizontal betatron cooling system. The minimum relative rms momentum spread obtained was  $\sigma_P/P = 4 \times 10^{-4}$  for a 4 GeV/c momentum beam. This corresponded to a rms spread in the center-of-mass energy ( $E_{cm} \equiv \sqrt{s}$ ) of the  $\bar{p}p$  system:

$$\sigma_{E_{cm}} = \frac{m_p}{E_{cm}} \times \beta_{\bar{p}} \times \sigma_P \approx 0.5 \text{ MeV} \quad (5)$$

Typical beam transverse dimensions were  $\sim 5$  mm in height and  $\sim 10$  mm

in width.

Phase displacement acceleration was used to change the beam energy during a resonance scan. The minimum step, obtained by a single RF sweep, corresponded to a beam momentum change of 3 to 6 MeV/c. Smaller energy drifts were obtained by appropriate changes in the momentum stochastic cooling system.

## 2.2 The Target

The choice of a molecular cluster gas-jet target[15] is a natural one for this kind of experiment: it can be operated in an accelerator environment and provides a well localized target with an appropriate density. The target built for the R704 experiment was operated at a density  $\rho_{H_2} = 1.0 \times 10^{14}$  atoms/cm<sup>3</sup> and had a thickness  $d_{H_2} = 0.9$  cm. This led to a maximum instantaneous luminosity:

$$\mathcal{L}_0 = \rho_{H_2} \times d_{H_2} \times N_{\bar{p}} \times f \text{ cm}^{-2} \text{ s}^{-1} = 3 \times 10^{30} \text{ cm}^{-2} \text{ s}^{-1} \quad (6)$$

where  $N_{\bar{p}}$  is the number of antiprotons circulating in the ring and  $f$  is their revolution frequency ( $f \approx 3.1 \times 10^5 \text{ Hz}$ ).

Figure 1 is a schematic of the target arrangement: we have, from left to right, the production stage, the accelerator beam pipe crossed by the jet, and the sink stage where the hydrogen is absorbed. The first element of the production stage is the expansion chamber, from which molecular hydrogen, kept at liquid nitrogen temperature ( $T_0 = 77^0 \text{ K}$ ) and at a typical pressure of 10 bar, escapes through a narrow-throat (30  $\mu\text{m}$ ), trumpet-like nozzle. In the adiabatic expansion large molecular clusters ( $10^4$  to  $10^6$  molecules per cluster) are formed in the jet core and flow at high speed ( $1290 \text{ m s}^{-1}$ ) over long distances in vacuum. The flow field is similar to that from a point source with almost straight streamlines. Downstream from the nozzle a three collimator system selects the central dense part of the jet.

Out of a total flux of  $10 \text{ torr} \times \text{liter s}^{-1}$  expanding from the nozzle, the collimator system selected a target beam of  $0.15 \text{ torr liter s}^{-1} = 10^{19} \text{ atoms s}^{-1}$ . A differential pumping system was used to remove the diffuse halo of hydrogen around the jet core. On the sink side the jet was dumped into a large cryogenic pump. During target operation the pressure increase in the beam vacuum pipe close to the target (caused by the breakup of clusters hitting the

walls of the last collimator) corresponded to  $\leq 1.5\%$  of the target thickness spread over a length of a few meters.

### 2.3 Beam Energy Measurements

The velocity of antiprotons circulating in a storage ring is related to their revolution frequency,  $f$ , and to the orbit length,  $L_{orb}$  by the equation:

$$v_{\bar{p}} = L_{orb} \times f \quad (7)$$

hence the beam total energy is:

$$E_{\bar{p}} = \frac{m_{\bar{p}}c^2}{\sqrt{[1 - (f \times L_{orb}/c)^2]}} \quad (8)$$

The beam revolution frequency spectrum can be determined by analyzing the beam current Schottky noise[16]. The spectral power density of the Schottky noise is proportional to the particle density at that frequency. The maximum in the frequency spectrum defines  $L_{orb}$  which must be determined independently.  $L_{orb}$  is the sum of the ring circumference (central orbit),  $L_0$ , and a correction term measuring displacements of the beam about  $L_0$ .

The momentum of the beam on the central orbit can also be determined from the measurement of the magnetic field in the bending dipoles ( $B_{dip}$ ):

$$P_{\bar{p}}(\text{GeV}/c) = 0.2997 \times B_{dip} \times \rho(\text{Tesla} \times \text{m}) \quad (9)$$

with  $\rho$  the dipoles' bending radius.

With equations (7) and (9) constraining the problem, it is then possible to determine the beam momentum by measuring only two of the three variables  $f$ ,  $B_{dip}$  and  $L_{orb}$ . The combination of observables chosen for a measurement is dictated by the operational characteristics of the storage ring in use.

In the ISR experiment the beam momentum was obtained by measuring the revolution frequency and the dipole field[17]. The error on this measurement was dominated by the error on the dipole field and was estimated to be  $\sigma_P = \pm 1.0 \text{ MeV}/c$ .

An absolute calibration of the beam energy was performed by analyzing the excitation curve obtained at the energy of formation of the  $J/\psi$ . The

energy of the antiproton beam ( $E_{\bar{p}}$ ) at the peak of the excitation curve is related to the mass of the  $J/\psi$  by Eqn.4 and the uncertainty on  $E_{\bar{p}}$  is:

$$\Delta E_{\bar{p}} = (M_{J/\psi}/m_{\bar{p}}) \times \Delta M_{J/\psi} \quad (10)$$

Since the mass of the  $J/\psi$  is known from independent measurements to within  $\sigma_{M_{J/\psi}} = \pm 100$  keV, the corresponding rms error on the beam energy is  $\sigma_{E_{\bar{p}}} = \pm 330$  keV. With these inputs, by inverting equation (10), one obtains the error on  $M_R$ :

$$\sigma_{M_R}(MeV) = [m_{\bar{p}}/M_R] \times \sqrt{\sigma_{E_p}^2 + [\sigma_P/\beta_{\bar{p}}]^2} \quad (11)$$

which, as an example, gives for  $M_{\chi_2} = 3.556 MeV/c^2$  an error  $\sigma_{M_R}(MeV) = 274 keV$ . To this systematic error one must add the statistical uncertainty in the determination of the energy of the peak of the excitation curve. This statistical component was by far the dominant one in the ISR experiment, which accumulated only  $\sim 3.0 pbarn^{-1}$  in the few months of data taking before the ISR was closed and turned into a storage ring for LEP magnets.

Despite its short lifetime, the R704 experiment reported measurements of the mass and width of the  $\chi_{1,2}$  states far superior to the existing ones from  $e^+e^-$  collider experiments and demonstrated the effectiveness of the method; a continuation of this line of experiments was called for.

## 2.4 The Fermilab Annihilation Source

The E760 experiment was proposed in 1985 to continue the study of charmonium states formed in  $\bar{p}p$  annihilations using the Accumulator of the Antiproton Source at Fermilab. The accumulator had been designed to store and cool 8.85 GeV/c antiprotons for the Tevatron collider operations. In order to provide antiprotons over the range of 3.5– 7.0 GeV/c for use in E760, the Accumulator had to be operated in a non-standard mode. First it was run in its design mode to accumulate the required number of antiprotons at 8.85 GeV/c. Then the  $\bar{p}$  beam was decelerated to the desired energy[18].

An RF cavity operating at the second harmonic of the beam revolution frequency ( $f \approx 0.62$  MHz) and with a maximum RF voltage amplitude of 3 kV was used to decelerate the beam. The deceleration process was controlled by an auxiliary front-end computer that set the current of magnets

as a function of beam momentum. These functions were determined experimentally at discrete points and interpolated linearly between these points. The deceleration proceeded at about 20 MeV/s.

After deceleration, the resonance was scanned by changing the beam energy in small steps. The smallest step size was determined by the least significant bit of digital control of the dipole power supply and corresponded to a beam momentum change of  $\sim 150$  keV/c. The main dipole and quadrupole power supplies were regulated to 1 part in  $10^5$  to ensure excellent stability of the beam orbit and energy.

The accumulator ring is equipped with powerful transverse and momentum stochastic cooling systems[19] which continuously compensated for the effects of multiple scattering and  $dE/dx$  loss in the target and in the residual gas in the ring. The momentum cooling narrowed the center-of-mass energy spread  $\sigma_{E_{cm}}$  to  $\sim 0.2$  MeV. A set of movable pick-up electrodes for momentum cooling made it possible to cool the beam at any chosen radial orbit position.

The internal hydrogen gas-jet target, of a design similar to the one used in the ISR experiment<sup>2</sup>, was operated at a typical density of  $0.6 \times 10^{14}$  atoms/cm<sup>3</sup> and had a diameter of 6.3 mm in the interaction region (for 95% containment). The antiproton beam had a diameter of  $\sim 5$  mm for 95% containment. The peak luminosity achieved was  $\sim 1.0 \times 10^{31}$  cm<sup>-2</sup>s<sup>-1</sup> with an antiproton beam of  $3.5 \times 10^{11}$   $\bar{p}$ 's. The beam lifetime was 50 to 90 hours depending on the energy of the beam and each store was used for about 1–2 lifetimes. In the case of  $J/\psi$  and  $\psi'$  formation runs the relatively high production cross sections made it possible to complete an energy scan of a resonance within a single store, while, at the other extreme, for low rate processes such as  $\bar{p}p \rightarrow \eta_c \rightarrow \gamma\gamma$  or  $\bar{p}p \rightarrow h_c \rightarrow J/\psi\pi^0$  data were accumulated at a single energy for the complete store.

In E760 the choice was made to determine the beam energy, by measuring the orbit length,  $L_{orb}$ , and the beam revolution frequency. From equation (8) we derive:

$$\Delta E_{\bar{p}} = m_{\bar{p}}c^2 \times \gamma_{\bar{p}}^3 \times \beta_{\bar{p}}^2 \times \left[ \left( \frac{\Delta f}{f} \right)^2 + \left( \frac{\Delta L_{orb}}{L_{orb}} \right)^2 \right]^{1/2} \quad (12)$$

The revolution frequency was measured very precisely, ( $\sigma_f/f \sim \pm 1.5 \times 10^{-7}$ ) and the error on  $E_{\bar{p}}$  was essentially due to the uncertainty in the measurement

---

<sup>2</sup>The E760 target used turbomolecular rather than cryogenic pumps.

of the orbit length,  $L_{orb}$ . The length of the central orbit,  $L_0$ , obtained from survey measurements was not accurate enough to determine the beam energy with the required precision. The choice was then made to calibrate the orbit length with the known mass of the  $\psi'$ .

The orbit length at the peak of the resonance is given by  $L_{orb} = c\beta/f$ , where  $f$  is measured at this orbit, and  $\beta$  is calculated from the  $\psi'$  mass. The error  $\Delta L_{orb}$  in the length of this reference orbit and the error in the reference mass  $\Delta M_R$  are related by the equation

$$\frac{\Delta L_{orb}}{L_{orb}} = \frac{M_R}{\gamma^3 \beta^2 m_p^2} \Delta M_R, \quad (13)$$

where we have neglected the contribution of the error in the beam frequency. The factor  $\gamma^3$  in the denominator justifies the choice of the  $\psi'$  for calibration, rather than the  $J/\psi$ , because for the higher mass state one obtains a better determination of the orbit length for the same  $\Delta M_R$ . The  $\pm 0.1$  MeV/ $c^2$  uncertainty in the published[20] mass of the  $\psi'$  corresponds to an uncertainty in the  $L_{orb}$  of  $\pm 0.67$  mm at the  $\psi'$ . An orbit length rms error of  $\sigma_{L_{orb}} = \pm 0.67$  mm in turn corresponds to  $\sigma_{M_R} = \pm 0.033$  MeV/ $c^2$  at the  $J/\psi$ .

Having established a reference orbit at the  $\psi'$ , one can determine the center-of-mass energy at the other resonances. If one could keep the beam on the reference orbit at all energies the only error in a measured mass would be the one discussed above. However, this situation cannot be achieved precisely over the entire energy range of the experiment. In general, the orbits used differed in length from the reference orbit by an amount  $\delta L$  ranging from +2 mm to -2 mm.

The difference between the reference orbit and the orbit used during a resonance scan was measured using 48 horizontal beam-position monitors<sup>3</sup> (BPM). The BPM readout, at the energy of interest, was compared to the BPM readout recorded at the reference energy. The resulting ‘‘difference orbit’’ was used to calculate  $\delta L$ . The error in the orbit length measurement was calculated[22] to be  $\pm 1$  mm and corresponded to a mass error at the  $J/\psi$ ,  $\sigma_{M_R} = \pm 0.05$  MeV/ $c^2$ . From these considerations the systematic error

---

<sup>3</sup>It should be mentioned that the reason why R704 chose to use  $B_{dip}$  rather than  $L_{orb}$  for their energy determination was that BPM measurements require a bunched beam. At the ISR the beam was bunched only for a short period after injection, at the lowest energy, while in the E760 experiment the beam could be totally or partially bunched at will at any energy.

Table 1: Comparison of annihilation source performance in R704 and E760.

	R704	E760
Maximum number of $\bar{p}$ stored	$1.1 \times 10^{11}$	$4.0 \times 10^{11}$
Jet density ( <i>atoms/cm</i> <sup>3</sup> )	$1.0 \times 10^{14}$	$0.6 \times 10^{14}$
Source dimensions (hor $\times$ vert $\times$ long) <i>cm</i> <sup>3</sup>	$1.0 \times 0.5 \times 0.9$	$0.5 \times 0.5 \times 0.6$
Maximum instantaneous luminosity ( <i>cm</i> <sup>-2</sup> <i>s</i> <sup>-1</sup> )	$3.0 \times 10^{30}$	$1.0 \times 10^{31}$
Minimum rms $E_{cm}$ spread (keV) at $E_{cm} = 4.0$ GeV	500	160
Error on $\chi_2$ mass from energy measurements (keV)	274	120

on the  $\chi_2$  mass for E760 is 120 keV, where contributions from  $\delta L$  and the mass uncertainty of the  $\psi'$  have been included. In Table 1 we compare the annihilation source performances for the two experiments.

### 3 EXPERIMENTAL TECHNIQUE

#### 3.1 Analysis of a Resonance Excitation Curve

The charmonium states are studied by sweeping the antiproton energy across a resonance  $R$  and measuring the cross section as a function of the beam energy. The resonance parameters are extracted by an analysis of the resulting excitation curve. The observed excitation curve is the convolution of the Breit-Wigner cross section for the resonance, with the energy distribution function of the beam, i.e.,

$$\sigma(E_{cm}) = \int_0^\infty \sigma_{BW}(E')G(E' - E_{cm}) dE', \quad (14)$$

where  $G(E)$  is the normalized beam-energy distribution function in the center-of-mass frame. The area under the resonance is given by

$$A = \int_0^\infty \sigma(E_{cm})dE_{cm} = \frac{\pi}{2}\sigma_{peak}\Gamma_R, \quad (15)$$

which is independent of the form of  $G(E)$ .  $\sigma_{peak}$  is the cross section at  $E_{cm} = M_R c^2$  given by

$$\sigma_{peak} = \frac{12\pi\hbar^2 B_{in}B_{out}}{(M_R^2 - 4m_p^2)c^2}. \quad (16)$$

Here  $B_{in}$  and  $B_{out}$  are the branching ratios ( $B = \Gamma_{partial}/\Gamma_R$ ) in the resonance formation channel ( $R \rightarrow \bar{p}p$ ) and in the decay channel respectively.

The resonance parameters to be extracted from a complete analysis of the excitation curve are: the mass  $M_R$ , the total width  $\Gamma_R$  and the product of branching ratios,  $B_{in} \times B_{out}$ . If  $G(E_{cm})$  is unknown, then the product  $\sigma_{peak}\Gamma_R$  can be obtained from the measured area. If  $G(E_{cm})$  is known, then  $\Gamma_R$  can be directly determined from the analysis of the shape of the measured excitation function, even if the resonance is substantially narrower than the center-of-mass energy distribution. With a beam width  $\Gamma_{E_{cm}}$  (FWHM)  $\approx 500$  keV (as was achieved in E760) a direct determination of  $\Gamma_R$  can be made from the analysis of the shape of the resonance excitation function even for the  $J/\psi$  resonance ( $\Gamma_R \approx 100$  keV). One can understand the reason for this sensitivity to such small resonance widths from the following considerations. For a beam energy distribution that is a Gaussian of width  $\Gamma_{E_{cm}} (= (8 \ln 2)^{1/2} \sigma_{E_{cm}})$ , the measured peak cross section  $\sigma_{peak}^*$  is

$$\sigma_{peak}^* = \sigma_{peak} \sqrt{\frac{\pi}{8}} \frac{\Gamma_R}{\sigma_{E_{cm}}} \exp\left(\frac{\Gamma_R^2}{8\sigma_{E_{cm}}^2}\right) \operatorname{erfc}\left(\frac{\Gamma_R}{\sqrt{8}\sigma_{E_{cm}}}\right), \quad (17)$$

where  $\operatorname{erfc}$  is the complementary error function. If  $\Gamma_{E_{cm}} > \Gamma_R$  it can be shown that

$$\frac{\sigma_{peak}^*}{A} \simeq \frac{0.94}{\Gamma_{E_{cm}}} \left[1 - 0.94 \frac{\Gamma_R}{\Gamma_{E_{cm}}}\right], \quad (18)$$

where 0.94 is the factor  $(4 \ln 2/\pi)^{1/2}$ . With  $\Gamma_R/\Gamma_{E_{cm}} \approx 0.2$  at the  $J/\psi$  a direct determination of  $\Gamma_R$  can still be obtained if  $\sigma_{peak}^*/A$  is measured.

The ratio  $\sigma_{peak}^*/A$  is independent of the efficiency and acceptance of the detector and of the absolute value of the luminosity, and  $\Gamma_R$  can be determined without having a detailed knowledge of these quantities. Stable running conditions, an accurate knowledge of the beam energy distribution function, and high statistical accuracy in the data are, however, necessary.

The measurement of the process

$$\bar{p}p \rightarrow (\bar{c}c) \rightarrow \bar{p}p \quad (19)$$

for any  $(\bar{c}c)$  charmonium state, would be very desirable since one can extract from the measurement of  $\sigma_{peak}$  a value of  $B_{\bar{p}p}$  ( $B_{in}B_{out} = B_{\bar{p}p}^2$ ). This measurement is not possible in our case since the process (19) competes with

a large background from  $\bar{p}p$  elastic scattering. It has been argued [21] that  $B(R \rightarrow \bar{p}p)$  could be extracted from a careful study of interference effects between the process of (19) and the elastic scattering process. This method has not yet been pursued, and one depends on measurements obtained from other experiments to extract separate values for  $B_{in}$  and  $B_{out}$ .

Interference between the amplitude for resonant production of a state and the amplitude for continuum, i.e. non-resonant, production of the same final state poses a problem in the case where the two processes are of comparable magnitude. Fortunately, for most of the charmonium states studied, the resonant production is much larger than the continuum and interference effects are negligible.

At each of the energy points where data were collected the measured number of events,  $n_i$ , was fitted to the expected number

$$\nu_i = \mathcal{L}_i(\sigma_{bkg} + \epsilon\sigma(E_{cm,i})), \quad (20)$$

where  $\sigma(E_{cm})$  is the cross section given by Eq. (14), and  $\sigma_{bkg}$  is the background cross section.  $\mathcal{L}_i$  is the luminosity for the data taken at the  $i$ 'th point, and  $\epsilon$  is the efficiency of the detector.

The two experiments, R704 and E760, followed similar strategies to extract the signal, evaluate the background level and monitor the source luminosity. The analysis of the center-of-mass energy distribution was improved in E760 to match the experiment goals. From now on, for simplicity, we will describe only the Fermilab experiment unless reference to R704 is called for.

## 3.2 Event Detection and Analysis

The rare events from direct formation of charmonium resonances were selected out of the large background of non-resonant  $\bar{p}p$  strong interactions by detecting their decays into  $e^+e^-$ , or, depending on the state quantum numbers, into  $\gamma\gamma$ . For higher ( $\bar{c}c$ ) excitations that do not decay directly into a two-body electromagnetic final state, it is still possible to obtain a strong signature by detecting their inclusive decay to  $J/\psi$  or  $\eta_c$ , which in turn decay into  $e^+e^-$  or two photons respectively.

The essential requirements for a detector are: (a) High efficiency for events with two large transverse momentum electrons (or photons) with the two particles roughly back to back, a requirement that implies either a symmetric

two-arm detector or a detector with full azimuthal coverage; (b) Excellent electron/hadron and  $\gamma/\pi^0$  discrimination and good energy and direction measurements for electrons and photons so that the mass of the decaying heavy charmonium states can be reconstructed accurately; (c) Hermeticity to reconstruct all events fully. Unfortunately, in these experiments, the gas jet target apparatus blocks a good fraction of the backward hemisphere and it is impossible to attain full coverage. It should be mentioned once more that the precision of the measurement of the final state does not influence the accuracy with which the ( $\bar{c}c$ ) resonances are measured (which is a function only of the uncertainty in the energy of the beam). A good reconstruction of the final state is, however, very useful in suppressing the background.

Both the R704 and E760 experiments followed these guidelines in the design of their detectors. In E760, the two-arm configuration of the R704 detector (Figure 2) was replaced by a cylindrical detector, (Figure 3) thereby increasing by a factor of approximately five the acceptance for events of interest.

The selection of events with a high mass  $e^+e^-$  in the final state was easily accomplished by identifying the electrons with the threshold gas Čerenkov counter, measuring their energy in the lead-glass central calorimeter (with  $\sigma_E/E = 6\%/\sqrt{E(\text{GeV})} + 1.4\%$ ) and their direction in the tracking system ( $\sigma_\theta \approx 4$  mrad and  $\sigma_\phi \approx 7$  mrad). The only remaining background originated from events where two electron pairs, coming from the Dalitz decays of  $\pi^0$  or from photon conversions in the beam pipe, simulated two isolated electron tracks in the detector and reconstructed to a high mass object. As an example of the results achieved, we show in Figure 4 the distribution of events as a function of the reconstructed invariant mass,  $m_{e^+e^-}$ , for data collected at the energy of formation of the  $\psi'$ , where the average rate is of approximately one event per inverse nanobarn of integrated luminosity. The large peak at the left arises from inclusive decays  $\psi' \rightarrow J/\psi + X \rightarrow e^+e^- + X$ , while the smaller peak at the higher mass is due to the exclusive decay  $\psi' \rightarrow e^+e^-$ . The shaded area represents the residual background estimated from the events collected outside the resonance region, at  $E_{cm} = 3666.7$  MeV.

The selection of events with a large-mass particle decaying to  $\gamma\gamma$  in the final state was more of a problem owing to the large residual background from  $\bar{p}p \rightarrow \pi^0\pi^0$  and  $\bar{p}p \rightarrow \pi^0\gamma$ . The worst type of background came from events with  $\pi^0$ 's decaying to an undetected low energy photon and to an

high-energy one, carrying almost all the energy of the parent  $\pi^0$ . To improve on background rejection the search was limited to  $2\gamma$  and  $3\gamma$  final states, accepting in the final selection only events fitting the exclusive processes  $\bar{p}p \rightarrow \gamma\gamma$  and  $\bar{p}p \rightarrow \eta_c + \gamma \rightarrow \gamma\gamma + \gamma$ .

### 3.3 Luminosity Measurement

The integrated luminosity for each energy setting was obtained by counting the number of recoil protons from  $\bar{p}p$  elastic scattering in a silicon detector located at  $\theta = 86.5^\circ$  from the beam direction. The value of the absolute luminosity was determined (with an estimated error of  $\sim 5\%$ ) using the known  $\bar{p}p$  elastic cross section, the detector acceptance, and the detector efficiency.

### 3.4 Determination of the Energy Spectrum

The beam energy spectrum is determined from the beam revolution frequency spectrum, through the relation

$$N_{\bar{p}}G(E_{cm}) = \frac{dN_{\bar{p}}}{dE_{cm}} = \frac{dN_{\bar{p}}}{df} \eta f \frac{E_{cm}}{\gamma\beta^2 m_p^2 c^2} \quad (21)$$

The factor  $\eta$  relates the momentum spread of the beam to the frequency spread of the beam:

$$\frac{dp}{p} = \frac{1}{\eta} \frac{df}{f} \quad (22)$$

and is defined as

$$\eta \equiv \frac{1}{\gamma^2} - \frac{1}{\gamma_t^2} \quad (23)$$

The transition energy gamma factor  $\gamma_t^2 \equiv (L_{orb}/p)(dp/dL)$  depends on the machine's magnetic lattice.

In order to derive the beam energy distribution it is important to determine  $dN_{\bar{p}}/df$ , and the  $\eta$  parameter of Eq. (21). The frequency spectrum  $dN_{\bar{p}}/df$  is determined very accurately by measuring the beam current Schottky noise. Three methods were used in E760 to estimate the value of  $\eta$ : the double-scan method, a method relying on the measurement of the beam synchrotron frequency, and a measurement of  $\gamma_t$  by changing the machine's

magnetic field and using the relation  $dB/B = \gamma_i^2 df/f$ . The most accurate value of  $\eta$  was derived from the double-scan method, which will be described later; the other two methods yielded consistent results.

The measured beam revolution frequency spectrum was very well parametrized over a wide range of frequencies with a “double Gaussian” function defined as two half-Gaussians joined at the peak. The width on the low-energy side was typically 10–20% wider than the high-energy side. A low-energy tail due to straggling usually contained less than 0.1% of the beam.

## 4 EXPERIMENTAL RESULTS

Most of our discussion will focus on the results from E760, which collected data for an integrated luminosity of  $\sim 30 \text{ pbarn}^{-1}$  during the summer of 1990 and the summer and fall of 1991, for a total period of nine months .

In section 4.1 we describe a set of new measurements of the parameters characterizing the  $J/\psi$  and  $\psi'$  resonances. These measurements provide a determination of the natural width of these narrow states, for the first time obtained directly from an analysis of the line shape. In section 4.2 we discuss the related measurement of the cross section for the continuum process  $\bar{p}p \rightarrow e^+e^-$  in the energy range:  $3.0 \leq E_{cm} \leq 3.6 \text{ GeV}$ . This measurement led to the first determination in this energy range of the proton electromagnetic form-factors in the time-like region.

Precise measurements on the  $\chi_1(^3P_1)$  and  $\chi_2(^3P_2)$  resonances and the discovery of the  $h_c(^1P_1)$  are presented in sections 4.3 and 4.4.

We conclude this review of the experimental results with a description of the measurements performed at the  $\eta_c$  and at the  $\chi_2$  formation energy by studying the reaction  $\bar{p}p \rightarrow \gamma\gamma$ , and of a search for the  $\eta'_c$  in the same channel.

### 4.1 The $J/\psi$ and the $\psi'$

Figure 5 shows an example of an excitation profile obtained from the measurement of the cross section for the inclusive process  $\bar{p}p \rightarrow J/\psi + \dots \rightarrow e^+e^- + \dots$  and for the exclusive process  $\bar{p}p \rightarrow e^+e^-$  at the  $\psi'$  formation energy[22], using antiprotons from a single store ( $\int L(t)dt \sim 1 \text{ pbarn}^{-1}$ ). The

dashed line represents the center-of-mass energy ( $E_{cm}$ ) distribution during this data taking, which had to be unfolded from the excitation curve to obtain the resonance profile. For states such as the  $J/\psi$  and the  $\psi'$ , where the resonance widths are comparable or smaller than the width of the center-of-mass energy distribution, one needs the high level of precision obtained from the double scan method[23] to determine the beam energy profile.

In a double scan, a resonance is scanned twice, once with the beam on the central orbit and another time with the beam on a side orbit, radially displaced from the central one. The frequency difference maintained between the two orbits was about one  $\sigma$  of the beam frequency spread. If the energy difference between the two orbits is known, then  $dE/df$  can be readily calculated. Since the peak of the resonance defines the energy of the beam, it can be used as a marker to measure the energy difference between the two orbits.

The double scan procedure is schematically illustrated in Figure 6. Data are first taken with the beam on the central orbit, and then the beam is decelerated to the side orbit, where more data are taken. The energy and frequency of the beam change, but the  $B$ -field is the same. The beam is then returned to the central orbit by changing the  $B$ -field but keeping the energy constant. The procedure is repeated several times across the resonance. The resulting cross section measurements can be plotted against the  $B$ -field, producing two excitation curves that are shifted with respect to each other as shown in Figure 6.

To obtain the quantity  $dE/df$ , where  $E$  is the beam energy, at constant  $B$ , one considers sets of points taken at the same magnetic field but on different orbits. The value of  $dE/df$  can be found, in essence, by forcing the excitation curve from the side orbit to match the central orbit curve. To be more specific, consider the data points of Figure 6. Points 2 and 3 are taken at the same  $B$ , and points 1 and 2 are the peaks of the two excitation curves. We have

$$(E_2 - E_3) = \frac{dE}{df}(f_2 - f_3), \quad (24)$$

and

$$(E_1 - E_3) = \beta^2 \gamma^3 m_p \frac{(f_1 - f_3)}{f_3}. \quad (25)$$

Since  $E_1$  and  $E_2$  are equal, from Eqs. (24) and (25) we get

$$\frac{dE}{df} = \beta^2 \gamma^3 m_p \frac{1}{f_3} \frac{(f_1 - f_3)}{(f_2 - f_3)}. \quad (26)$$

Equivalently,  $\eta$ , as defined in Eq. (21), is

$$\eta = \frac{1}{\gamma^2} \frac{(f_2 - f_3)}{(f_1 - f_3)}. \quad (27)$$

We see from Eqs. (26) and (27) that  $dE/df$  or  $\eta$  can be determined accurately by this method because it depends only on frequency measurements; the parameters in the equations ( $\beta$  and  $\gamma$ ) are known accurately because the resonance masses of  $J/\psi$  and  $\psi'$  are themselves accurately known[20]. Variations in the orbit length for the data points on the same ( central or side) orbits introduce a negligible uncertainty.

For the analysis of these narrow resonances,  $\sigma_{BW}$  in Eq. (14) has been modified to include the effect of radiation from the initial  $\bar{p}p$  state[24]. This effect, although small, decreases the width  $\Gamma_R$  of  $J/\psi$  and  $\psi'$  by about 10 keV and 2 keV, respectively. The resonance mass  $M_R$  is not affected. For the  $J/\psi$ , the interference between the resonant amplitude and the continuum amplitude[25] for  $\bar{p}p \rightarrow e^+e^-$  is also considered, but is found not to change the results significantly. The background for the resonance fitting procedure is determined from off-resonance runs.

Figure 7 shows the results of the double-scan running for the  $J/\psi$  and the  $\psi'$  from E760. From the fit to these data, the mass of the  $J/\psi$  and the total widths and product of branching ratios to  $p\bar{p}$  and  $e^+e^-$  for both  $J/\psi$  and  $\psi'$  were determined. These results are summarized in Table 2.

The mass of the  $J/\psi$  was determined by E760 to be  $M_{J/\psi} = 3096.87 \pm 0.03(\text{stat.}) \pm 0.03(\text{sys.})\text{MeV}/c^2$ . This represents a small improvement over earlier measurements. For the determination of the branching ratios the experimenters had to unfold the effects of detector efficiency and geometrical acceptance of their apparatus; this last measurement also depends on the absolute value of the luminosity.

Table 2:  $J/\psi$  and  $\psi'$  results from E760.

	Width(keV)	$B_{in}B_{out}^a$	$B(\bar{p}p)^b$
$J/\psi$	$99 \pm 12 \pm 6$	$(1.14_{-.12}^{+.16} \pm .10) \times 10^{-4}$	$(1.82_{-.19}^{+.26} \pm .16 \pm .06) \times 10^{-3}$
$\psi'$	$306 \pm 36 \pm 16$	$(1.17_{-.12}^{+.14} \pm .08) \times 10^{-5}$	$(2.61_{-.27}^{+.31} \pm .17 \pm .17) \times 10^{-4}$

<sup>a</sup>  $B_{in}B_{out} = B(J/\psi \rightarrow \bar{p}p) B(J/\psi \rightarrow e^+e^-)$  for the  $J/\psi$ , and  
 $B_{in}B_{out} = B(\psi' \rightarrow \bar{p}p) [B(\psi' \rightarrow e^+e^-) + B(\psi' \rightarrow J/\psi X)B(J/\psi \rightarrow e^+e^-)]$  for the  $\psi'$ .  
The errors, in the order shown, are statistical and systematic.

<sup>b</sup> Using  $B(J/\psi \rightarrow e^+e^-)$ ,  $B(\psi' \rightarrow e^+e^-)$ , and  $B(\psi' \rightarrow J/\psi + X)$  from Ref. [20].  
The errors, in the order shown, are statistical, systematic, and due to the errors in the branching ratios from Ref. [20].

## 4.2 An aside: The Proton Electromagnetic Form Factor

The reaction  $p\bar{p} \rightarrow e^+e^-$  was also studied at other energies, where there is no resonant production of the  $e^+e^-$  state, to measure the proton's electromagnetic form factor in the time-like region. The differential cross section for this process is given in terms of the proton magnetic and electric form factors by:

$$\frac{d\sigma}{d(\cos \theta^*)} = \frac{\pi\alpha^2(\hbar c)^2}{8EP} \times [ |G_M|^2(1 + \cos^2\theta^*) + \frac{4m_p^2}{s} |G_E|^2 \sin^2\theta^* ] , \quad (28)$$

with  $E$  and  $P$  the center-of-mass energy and momentum of the antiproton, and  $\theta^*$  the angle between the  $e^-$  and the  $\bar{p}$  in the center-of-mass system. Since the data samples used in such a study are small and cover a limited angular range, the value of  $|G_M|$  is obtained under the assumption that  $|G_E| = |G_M|$ .

E760 has reported measurements[25] of the proton form factor at  $E_{cm} = 3.0, 3.5,$  and  $3.6$  GeV, while R704 was able to set only upper limits[26] in the same energy range. These results, together with measurements at lower energies, are shown in Figure 8 in the form of  $q^4|G_M|/\mu_p$  vs.  $-q^2 = s/c^2$  ( $\mu_p = 2.793$  is the magnitude of the proton's magnetic moment). It is seen that the data for  $-q^2 > 5(\text{GeV}/c)^2$  follow the perturbative QCD prediction[27]

for large momentum transfers, i.e., that  $G_M(q^2) \propto q^{-4} \alpha_s^2(q^2)$ , where the running strong coupling-constant  $\alpha_s$  is proportional to  $1/\ln(q^2/\Lambda^2)$  with  $\Lambda = 0.2$  GeV.

As an interesting aside, from the fit shown in Figure 8, one can deduce the value of the cross section for the process  $\sigma(e^+e^- \rightarrow \gamma^* \rightarrow p\bar{p})$ , at energies near the  $J/\psi$  and  $\psi'$  mass. From experiments carried out in  $e^+e^-$  colliders[28] the cross section for the similar process  $\sigma(e^+e^- \rightarrow \gamma^* \rightarrow \text{hadrons})$  can also be determined. Thus, the branching fractions

$$f(\gamma^*) \equiv \frac{\sigma(e^+e^- \rightarrow \gamma^* \rightarrow p\bar{p})}{\sigma(e^+e^- \rightarrow \gamma^* \rightarrow \text{hadrons})} \quad (29)$$

are found to be  $(2.6 \pm 0.5) \times 10^{-4}$  at the  $J/\psi$ , and  $(0.52 \pm 0.09) \times 10^{-4}$  at the  $\psi'$ . The equivalent fractions for gluonic decays of the  $J/\psi$  and the  $\psi'$ , where the decay proceeds through an intermediate three-gluon state, i.e.,

$$f(ggg) \equiv \frac{\Gamma(^3S_1 \rightarrow ggg \rightarrow p\bar{p})}{\Gamma(^3S_1 \rightarrow ggg \rightarrow \text{hadrons})} \quad (30)$$

are estimated to be  $(31 \pm 2) \times 10^{-4}$  for the  $J/\psi$ , and  $(12 \pm 4) \times 10^{-4}$  for the  $\psi'$ . This leads to the purely experimental result that hadronization via gluons favors the  $p\bar{p}$  channel by approximately an order of magnitude as compared to hadronization via one photon.

### 4.3 The $1^3P_J$ Triplet

The study of the production of the  $\chi_{c1}$  and  $\chi_{c2}$  charmonium states was carried out in a fashion similar to the one used in the study of the  $J/\psi$  and  $\psi'$  resonances. The reactions studied are:

$$p\bar{p} \rightarrow \chi_{c1,2} \rightarrow J/\psi \gamma \rightarrow e^+e^- \gamma \quad (31)$$

The excitation curves obtained by the R704 experiment[29] are shown in Figure 9, together with the mass spectra obtained by the Crystal Ball experiment at SPEAR[30]. This serves as a graphic illustration of the advantage of the  $p\bar{p}$  annihilation technique. The resolution of R704, determined only by the beam energy resolution, is far superior to that of the Crystal Ball detector. Figure 10 shows the excitation curves obtained by E760, where the center-of-mass energy resolution is also indicated as a dotted line[31],[32].

A fit to the excitation curves yields the values of the masses and total widths shown in table 3 and also, after correcting for detector efficiencies and geometrical acceptances, the values for the product  $\Gamma(\chi_{c1,2} \rightarrow p\bar{p})B(\chi_{c1,2} \rightarrow J/\psi \gamma)B(J/\psi \rightarrow e^+e^-)$ . The widths measured by E760 are more accurate than the R704 measurement, a result of the higher number of events in E760 (e.g. 559 events at the  $\chi_{c2}$  for E760 as compared to 50 events for R704). We also note that both masses measured by R704 are 0.8 MeV/c<sup>2</sup> higher than the masses measured in E760; this could indicate a small error in the absolute mass scale in one of the experiments. E760 has used both the  $J/\psi$  and the  $\psi'$  masses as energy calibration points, thus spanning the range of the  $\chi_c$  masses, while R704 used only the  $J/\psi$  mass as a calibration point.

The width of the  $\chi_{c0}$  is a quantity of considerable interest, since perturbative QCD calculations directly relate it to the width of the  $\chi_{c2}$ . Unfortunately, the  $\chi_{c0}$  has not been studied by either of the two experiments because this state does not decay readily into  $J/\psi$  ( $B(\chi_{c0} \rightarrow \gamma J/\psi) = (6.6 \pm 1.8) \times 10^{-3}$  [20]).

#### 4.3.1 Angular Distributions in $\chi_{c2}$ Decays

The study of the angular distributions for the process

$$p\bar{p} \rightarrow \chi_{c2} \rightarrow J/\psi \gamma \rightarrow e^+e^- \gamma \quad (32)$$

allows for an evaluation of the contributions of quadrupole and octupole transitions to this radiative decay.

The angular distribution is described in terms of five helicity amplitudes:  $B_0, B_1, a_1, a_2,$  and  $a_3$ . Unitarity constraints allow for only three independent amplitudes, taken to be  $B_0$ , which describes the dynamics of  $\chi_{c2}$  formation, and  $a_2, a_3$ , which correspond to the contribution of magnetic quadrupole and electric octupole transitions in the  $\chi_{c2}$  decay, respectively.  $a_1$  characterizes the electric dipole component of the decay.

$B_0$  is expected to be zero in the massless QCD limit, and  $a_3$  is expected to be zero under the hypothesis that a single quark is involved in the radiative transition. Indeed, both the E760[33] and R704[34] analyses yield non-zero values only for  $a_2$ , but of different signs. The E760 result ( $-0.14 \pm 0.06$ ) thus resolves the outstanding discrepancy in the sign of  $a_2$  between the measurement of R704 ( $+0.46^{+0.19}_{-0.18}$ ) and the value obtained from the study of  $e^+e^- \rightarrow \chi_{c2} \rightarrow J/\psi \gamma$  by the Crystal Ball experiment[35] ( $-0.33^{+0.12}_{-0.29}$ ). Given

Table 3:  $\chi_{c1}$  and  $\chi_{c2}$  masses, widths, and branching ratios

Parameter	R704 Result	E760 Result	World Average <sup>a</sup>
$M(\chi_{c1})$ (MeV/c <sup>2</sup> )	$3511.3 \pm 0.4 \pm 0.4$	$3510.53 \pm 0.04 \pm 0.12$	$3510.53 \pm 0.13$
$\Gamma_{total}(\chi_{c1})$ (MeV)	$< 1.3$	$0.88 \pm 0.11 \pm 0.08$	$0.88 \pm 0.14$
$\Gamma(\chi_{c1} \rightarrow p\bar{p}) \times$ $B(\chi_{c1} \rightarrow J/\psi \gamma) \times$ $B(J/\psi \rightarrow e^+e^-)$ (eV)	$1.18_{-0.24}^{+0.26}$	$1.29 \pm 0.09 \pm 0.13$	
$\Gamma(\chi_{c1} \rightarrow p\bar{p})$ (eV)			$76 \pm 16$
$B(\chi_{c1} \rightarrow p\bar{p}) \times 10^4$			$0.86 \pm 0.12$
$M(\chi_{c2})$ (MeV/c <sup>2</sup> )	$3556.9 \pm 0.4 \pm 0.5$	$3556.15 \pm 0.07 \pm 0.12$	$3556.17 \pm 0.13$
$\Gamma_{total}(\chi_{c2})$ (MeV)	$2.6_{-1.0}^{+1.4}$	$1.98 \pm 0.17 \pm 0.07$	$2.00 \pm 0.18$
$\Gamma(\chi_{c2} \rightarrow p\bar{p}) \times$ $B(\chi_{c2} \rightarrow J/\psi \gamma) \times$ $B(J/\psi \rightarrow e^+e^-)$ (eV)	$2.14_{-0.41}^{+0.47}$	$1.67 \pm 0.09 \pm 0.1$	
$\Gamma(\chi_{c2} \rightarrow p\bar{p})$ (eV)			$200 \pm 27$
$B(\chi_{c2} \rightarrow p\bar{p}) \times 10^4$			$1.0 \pm 0.1$

Where two errors are shown the first is statistical and the second systematic.

<sup>a</sup> Using the values from reference [20].

the value of  $a_2$  obtained by E760, one extracts a value for the anomalous magnetic moment of the charmed quark:  $\kappa_c = 0.46 \pm 0.62 \pm 0.37$ , where the first error reflects the measurement uncertainties in  $a_2$ , while the second reflects theoretical uncertainties in relating  $a_2$  to  $\kappa_c$ .

#### 4.4 The ‘Missing’ $1^1P_1$

The singlet states of charmonium (e.g., the  $\eta_c[1^1S_0, J^{PC} = 0^{-+}]$ ,  $\eta'_c[2^1S_0, J^{PC} = 0^{-+}]$ ,  $h_c[1^1P_1, J^{PC} = 1^{+-}]$ ) pose an unusual experimental challenge because they can neither be resonantly produced in  $e^+e^-$  annihilation into a virtual photon ( $J^{PC} = 1^{--}$ ) nor be populated by E1 radiative decays of the  $^3S_1$  states (i.e., the  $J/\psi[1^3S_1, J^{PC} = 1^{--}]$  and the  $\psi'[2^3S_1, J^{PC} = 1^{--}]$ ). Indeed, until quite recently only the  $\eta_c$  had been positively identified. One of the major objectives of the experiments studying charmonium production in  $p\bar{p}$  annihilation has been to study these elusive states, and in particular to search for the  $h_c$ . The observation of this state is important not only because it is the last unidentified  $n = 1$  state of charmonium, but also because a comparison of its mass with the center-of-gravity mass of the three triplet  $^3P$  states

$$m_{cog} = \frac{\sum_J (2J + 1) m_{\chi_{cJ}}}{\sum_J (2J + 1)} \quad (33)$$

provides a measurement of the deviation of the vector part of the quark-antiquark interaction from pure one gluon exchange. In addition, the branching ratios of the  $h_c$  hadronic decays relate to the validity of QCD helicity selection rules, QCD multipole expansion models, and isospin conservation.

The  $h_c$  can be formed in  $p\bar{p}$  through the annihilation of the initial state particles into three gluons. It is expected to have a small width ( $< 1$  MeV) and decay with comparable rates to hadrons, and radiatively, through an electric dipole transition, to the  $\eta_c\gamma$  final state. The cross section at the peak of the resonance for the process  $p\bar{p} \rightarrow h_c$  is expected to be less than  $10^{-6}$  of the total cross section for  $p\bar{p} \rightarrow$  hadrons.

R704 performed a search by looking for the inclusive decays :

$$h_c \rightarrow J/\psi X \rightarrow e^+e^- X \quad . \quad (34)$$

E760 searched[36] for the  $h_c$  by focusing on the decays :

$$h_c \rightarrow \eta_c \gamma \rightarrow \gamma\gamma \gamma \quad (35)$$

$$h_c \rightarrow J/\psi \pi^0 \rightarrow e^+ e^- \pi^0 \quad (36)$$

$$h_c \rightarrow J/\psi 2\pi \rightarrow e^+ e^- 2\pi \quad (37)$$

E760 collected data in 0.5 MeV steps near the center of gravity of the  $\chi$  states. The final state for process (35) is hard to detect owing to the very small branching ratio of the decay  $\eta_c \rightarrow \gamma\gamma$ . No significant signal was seen by E760 in this mode. The other two modes they searched for are expected to have small branching ratios, but the  $J/\psi$  in the final state provides a very distinctive signature. Figure 11 shows the invariant mass distribution for  $e^+e^-$  pairs for all the data taken during their  $h_c$  scan. A clear peak at the  $J/\psi$  shows that events of the type  $p\bar{p} \rightarrow J/\psi X$  were indeed observed.

Events with  $m_{e^+e^-}$  larger than 2.9 GeV/c<sup>2</sup> were fitted to the reactions  $p\bar{p} \rightarrow J/\psi \pi^0$ ,  $p\bar{p} \rightarrow J/\psi 2\pi$ ,  $p\bar{p} \rightarrow J/\psi \gamma$ , and  $p\bar{p} \rightarrow e^+e^-$  whenever the event topology was compatible with the final state hypothesis. Most of the events could be unambiguously identified as either  $J/\psi \gamma$  (cross hatched area in Figure 11), or  $J/\psi \pi^0$  (solid area), while a few events were identified as  $p\bar{p} \rightarrow e^+e^-$  (vertically striped area). No events were found that could fit the final states  $J/\psi \pi^0 \pi^0$ , or  $J/\psi \pi^+ \pi^-$ . The  $J/\psi \gamma$  events can be explained as background expected from the tails of the nearby  $\chi_{c1}$  and  $\chi_{c2}$  resonances.

Figure 12(a) shows the cross section as a function of center-of-mass energy for the reaction  $p\bar{p} \rightarrow J/\psi \pi^0 \rightarrow (e^+e^-) \pi^0$ . The data, binned in intervals of 150 keV in the center-of-mass energy, show for energies below  $E_{cog}$  a uniform level of cross section of  $\sigma(p\bar{p} \rightarrow J/\psi \pi^0) = 99 \pm 40$  pbarn, which is in reasonable agreement with the prediction for this continuum process[38]. Above  $E_{cog}$  there is an enhancement around 3526 MeV which can be fitted to a resonance of mass  $M = 3526.2 \pm 0.15 \pm 0.20$  MeV/c<sup>2</sup> and has a width compatible with the beam energy resolution. The upper limit to the width is  $\Gamma < 1.1$  MeV at the 90% confidence level<sup>4</sup>. The probability that this peak is a fluctuation of the flat continuum is 1/400. E760 interpreted this structure to be the  $h_c(1^1P_1)$  state of charmonium, a presumptive interpretation supported by the decay mode and by the close proximity of the mass to  $M_{cog} = 3525.27 \pm 0.12$  MeV.

The branching ratio product  $B(h_c \rightarrow p\bar{p})B(h_c \rightarrow J/\psi \pi^0)$  can range from  $(1.7 \pm 0.4) \times 10^{-7}$  to  $(2.3 \pm 0.6) \times 10^{-7}$ . The lack of any events of the class

<sup>4</sup>Because of the limited statistics the analysis ignored the effects of possible interference between the resonance and the continuum.

$p\bar{p} \rightarrow J/\psi 2\pi$  sets a limit to the ratio  $B(h_c \rightarrow J/\psi 2\pi)/B(h_c \rightarrow J/\psi \pi^0) < 0.18$  at the 90% confidence level.

R704 observed[37] 5 events consistent with process (34) at a mass of  $3525.4 \pm 0.8 \pm 0.5 \text{ MeV}/c^2$ . They obtain a value for  $\Gamma_{h_c} \times B(h_c \rightarrow p\bar{p}) \times B(h_c \rightarrow J/\psi X) \times B(J/\psi \rightarrow e^+e^-)$  of  $0.135^{+0.150}_{-0.060} \text{ eV}$ , while the same quantity determined by E760 is  $0.010 \pm 0.003 \text{ eV}$ . The data from the two experiments are compared in Figure 12, where the R704 data have been shifted in energy by  $-0.8 \text{ MeV}$  to account for the systematic energy scale difference between the two experiments noted in section 4.3. The R704 events correspond to a rate which is ten times higher than the cross section measured by E760 and must be presumed to be dominated by background.

## 4.5 The $\bar{p}p \rightarrow (\bar{c}c) \rightarrow \gamma\gamma$ Process

Both R704 and E760 studied the  $\eta_c(1^1S_0)$  and the  $\chi_{c2}(1^3P_2)$  states through the reaction:

$$\bar{p} + p \rightarrow (\bar{c}c) \rightarrow \gamma + \gamma \quad (38)$$

The study of this process allows the determination of  $\Gamma_{\gamma\gamma} \times B(R \rightarrow p\bar{p})$  and  $B(R \rightarrow \bar{p}p) \times B(R \rightarrow \gamma\gamma)$ . The derived values for  $B(R \rightarrow \gamma\gamma)$  and for the resonance partial width into two photons,  $\Gamma_{\gamma\gamma}$  probe the physics of short distance annihilation processes. The E760 collaboration also searched for the formation of the  $\eta'_c(2^1S_0)$  resonance in the same process.

### 4.5.1 Study of the $\eta_c$

The cross sections for the process  $\bar{p}p \rightarrow \gamma\gamma$  as a function of the center-of-mass energy in the  $\eta_c$  region as measured[39] by E760 is shown in Figure 13. A structure is seen in the mass region around  $2990 \text{ MeV}/c^2$  above a background of comparable magnitude.

The data were fit with the maximum likelihood method to a smooth background plus a Breit-Wigner line shape. The background cross section was adequately parametrized with a power law:

$$\sigma_{back} = A \times (2988/E_{cm})^B \quad (39)$$

This background is due predominantly to misidentified  $\pi^0\pi^0$  and  $\pi^0\gamma$  events but the presence of a small component of genuine non-resonant  $\bar{p}p \rightarrow \gamma\gamma$

events could not be excluded. The analysis of the data assumes complete incoherence between signal and background, and could lead to misleading results in the presence of interference effects between the amplitude for resonant production and the amplitude for the non-resonant continuum. The data sample is unfortunately too small to allow for a more general analysis.

The values for  $M_{\eta_c}$  obtained by E760 and R704[40] are  $2987.5^{+3.0}_{-2.8} \text{ MeV}/c^2$  and  $2982.6^{+2.7}_{-2.3} \text{ MeV}/c^2$ , respectively, to be compared with the world average[20] of  $2978.8 \pm 1.9 \text{ MeV}/c^2$ . Values for  $\Gamma_{\gamma\gamma}, B(\eta_c \rightarrow \bar{p}p)$ , and  $B(\eta_c \rightarrow \gamma\gamma) \times B(\eta_c \rightarrow \bar{p}p)$  from E760 and R704 are compared in Table 4 to results from other recent experiments and to theoretical predictions.

#### 4.5.2 Measurement of the Decay Rate for $\chi_2 \rightarrow \gamma\gamma$ , and a Search for the $\eta'_c$

Figure 14 shows the yield of  $\bar{p}p \rightarrow \gamma\gamma$  events collected[39],[50] by E760 in the range  $3520 \leq E_{cm} \leq 3690 \text{ MeV}$ , where 1P and 2S charmonium resonances are formed. A four  $\sigma$  excess over background is evident at 3556 MeV, the energy of formation for the  $\chi_{c2}$ . This event excess, fitted with a Breit-Wigner distribution of the  $\chi_{c2}$  mass and width, gives for the product of branching ratios  $B(\chi_2 \rightarrow \bar{p}p) \times B(\chi_2 \rightarrow \gamma\gamma) = (1.60 \pm 0.39 \pm 0.16) \times 10^{-8}$ . Using the values of  $\Gamma_{\chi_2}$  and  $B(\chi_2 \rightarrow \bar{p}p)$  from the same experiment, one derives the values of  $B(\chi_2 \rightarrow \gamma\gamma)$  and of the partial decay width to  $\gamma\gamma$ . These are compared to results from  $e^+e^-$  experiments in Tab.5, which also includes the values obtained by R704[40].

The energy range spanned by these data overlaps with the mass region where the  $\eta'_c$  was observed by the Crystal Ball experiment[55]. Upper limits for the product  $B(\eta'_c \rightarrow \bar{p}p)B(\eta'_c \rightarrow \gamma\gamma)$ , for various values of  $\Gamma_{\eta'_c}$ , as determined by E760, are shown in Figure 15. The lack of any enhancement in that region is taken as an indication that a more systematic and higher sensitivity search for the  $\eta'_c$  must be performed. In this respect we can look with some optimism to the future data taking of the E835 experiment, the continuation of E760.

Table 4:  $\eta_c$  Widths and Branching Ratios.

	$B(\eta_c \rightarrow \gamma\gamma) \times B(\eta_c \rightarrow \bar{p}p)$ in units of $10^{-8}$	$B(\eta_c \rightarrow \gamma\gamma)$ in units of $10^{-4}$	$\Gamma(\eta_c \rightarrow \gamma\gamma)$ keV
Experiment			
E760 [39]	$35.4 \pm 7.6$	$3.0 \pm 0.7 \pm 1.0^a$	$7.0_{-2.0}^{+2.9} \pm 2.3^a$
R704 [40]	$68_{-31}^{+42}$		
CLEO [41]			$5.7 \pm 1.8 \pm 1.6$
TPC [42]			$6.4_{-3.4}^{+5.0}$
PLUTO [43]			$33_{-12}^{+15} \pm 9^b$
TASSO [44]			$19.9 \pm 6.1 \pm 8.6$
ARGUS [45]			$12.2 \pm 3.0$
L3 [46]			$8.0 \pm 2.3 \pm 2.4$
Theory			
PQCD [47] <sup>c</sup>		$3.1_{-0.4}^{+0.5}$	
B.A. [48][49]			$3 \div 5$

<sup>a</sup> Using the Particle Data Group[20] value  $B(\eta_c \rightarrow \bar{p}p) = (12 \pm 4) \times 10^{-4}$ . The first errors quoted come from the E760 measurement while the second ones reflect the uncertainties in the values taken from other experiments.

<sup>b</sup> Value calculated from the PLUTO measurement of  $B(\eta_c \rightarrow K_S K^\pm \pi^\mp) \times B(\eta_c \rightarrow \gamma\gamma)$ , using the Particle Data Group[20] value  $B(\eta_c \rightarrow K \bar{K} \pi) = (6.6 \pm 1.8) \times 10^{-2}$ . The first error quoted comes from the PLUTO measurement while the second ones reflects the uncertainties in  $B(\eta_c \rightarrow K \bar{K} \pi)$ .

<sup>c</sup> Using the value  $\alpha_s(m_c) = 0.276 \pm 0.014$ [47]. The error quoted is due only to the uncertainty in the value of  $\alpha_s$ .

Table 5:  $\chi_{c2} \rightarrow \gamma\gamma$  Width and Branching Ratio.

	$\Gamma(\chi_{c2} \rightarrow \gamma\gamma)$ (keV)	$B(\chi_{c2} \rightarrow \gamma\gamma)$ ( $10^{-4}$ )
<b>Experiment</b>		
E760 [50]	$0.32 \pm 0.08 \pm 0.05$	$1.6 \pm 0.4 \pm 0.2$
R704 [40]	$2.9_{-1.0}^{+1.3} \pm 1.7^a$	$11_{-4}^{+5} \pm 4^a$
CLEO [41]	$< 1.0$ (95% C.L.)	
VENUS [51]	$< 4.2$ (95% C.L.)	
TPC [42]	$< 4.2$ (95% C.L.)	
Crystal Ball [52]	$2.8 \pm 2.0$	
DASP [20][53]	$< 1.6$ (90% C.L.)	
<b>Theory</b>		
PQCD [47]	$0.81 \pm 0.15^b$	
B.A. [49]	0.56	
B.B.L. [54]		$4.1 \pm 1.1(\pm 36\%)$

<sup>a</sup> Assuming isotropic angular distribution and  $\Gamma(\chi_{c2}) = 2.6_{-1.0}^{+1.4} \text{ MeV}$ .

<sup>b</sup> Using  $\Gamma(\chi_{c2} \rightarrow gg) = 1.71 \pm 0.21 \text{ MeV}$  and  $\alpha_s = 0.276 \pm 0.014$ .

## 5 INTERPRETATION OF THE EXPERIMENTAL RESULTS

Precise measurements of the quarkonium states can in principle lead to the determination of the fundamental parameters of quantum chromodynamics, the mass of the constituent quarks and the coupling constant of strong interactions, just as the study of positronium and of the hydrogen atom are sufficient to derive the mass of the electron and the fine-structure coupling constant.

In this section we will first review briefly some aspects of charmonium phenomenology (5.1 and 5.2) and then discuss in 5.3 attempts to derive the parameters of the theory from the experimental results presented in this review.

### 5.1 Charmonium Dynamics

Charmonium, the bound system of a charmed quark and its antiquark, should in principle be completely described within the framework of QCD. While such a description has not yet been achieved, significant progress has been made along two approaches: one is through lattice QCD, and the other is through potential models.

Lattice calculations[6] start from the Lagrangian of QCD and attempt to solve the equations of motion numerically on a discrete lattice of space-time points and to extract physically meaningful quantities by taking the appropriate limit (e.g. small lattice spacing). In principle this approach should be exact, but in practice lattice QCD calculations still need to make simplifying assumptions and have not yet reached the point of completely describing charmonium. Nevertheless, certain quantities can be reliably calculated by this technique[56], e.g. the level spacing between the  $1P$  and  $1S$  states as a function of the strong coupling constant. This calculation has been used to determine the value of the strong coupling constant from the observed level spacing. Given the mass measurements for the  $\eta_c$ ,  $J/\psi$ ,  $h_c$ , and the  $\chi_c$ 's from the  $p\bar{p}$  and  $e^+e^-$  experiments the value of  $\alpha_{\overline{MS}}(5GeV) = 0.174 \pm 0.012$  is obtained. Equivalently,  $\Lambda_{\overline{MS}}^{(4)} = 160_{-37}^{+47} MeV$  or, by extrapolating to the mass of the  $Z$ ,  $\alpha_{\overline{MS}}(M_Z) = 0.105 \pm 0.004$  a value with comparable accuracy to the one obtained in high energy  $e^+e^-$  experiments.

In the potential model approach[5] [57] a phenomenological potential  $V(r)$  is used to describe the interaction between the  $c$  and  $\bar{c}$  quarks. Since the radius of the system,  $r_B = (\frac{2}{3}\alpha_s m_c)^{-1} \approx 1$  fermi, is large the effects of strong long-range binding forces have to be included, i.e. the interaction has to become strong at large separation. The funnel potential  $V(r) = a/r + kr$  provides a simple example of a QCD-inspired potential. The coulomb-like term describes the short distance behaviour as expected for one-gluon exchange, with “a” proportional to the running coupling constant ( $a = -\frac{4}{3}\alpha_s(r)$ ). The constant  $k \approx 0.15 \text{ GeV}^2$  in the confining term measures the string tension. Other functional forms for the potential have been used in the literature; the spin-averaged level structure is quite insensitive to the form used provided some general conditions ( $\nabla^2 V(r) > 0$  and  $\frac{d}{dr} \frac{1}{r} \frac{dV(r)}{dr} < 0$  [58]) are satisfied which are required for the correct ordering of the levels.

The potential  $V(r)$  may include terms arising from the most general spin structure of the quark-antiquark interaction (scalar, vector, axial vector, pseudoscalar and tensor), but the existence of pseudoscalar and vector charmonium states imply that the dominant terms are due to vector and scalar exchange. Perturbation theory shows that the short distance part of the potential is dominated by single gluon, therefore vector, exchange, while the level spacing of the  $\chi_c$  states and results obtained by lattice QCD [59] suggest that the long-range confining potential is predominantly due to an effective scalar exchange.

Starting from a central potential  $V(r)$ , the Breit-Fermi hamiltonian of a system of two interacting fermions of equal mass, containing relativistic corrections up to order  $v^2/c^2$ , is derived<sup>5</sup>. This approximation is acceptable since in the  $(c\bar{c})$  system typical velocities for the two quarks are  $v/c \sim 0.5$ . The Breit-Fermi hamiltonian is :

$$H = H_0 + H_1 = [2m + p^2/m - p^4/(4m^3) + V(r)] + [H_{SI} + H_{LS} + H_T + H_{SS}] \quad (40)$$

where the term  $H_1$  (with  $H_1 \ll H_0$ ) includes, besides the spin-independent part  $H_{SI}$ , terms that describe the spin-orbit interaction :

$$H_{LS} = \vec{L} \cdot (\vec{S}_1 + \vec{S}_2) \frac{1}{2m^2 r} (3V'_v - V'_s) \quad (41)$$

---

<sup>5</sup>The Breit-Fermi hamiltonian has been derived from the static non-relativistic reduction [60] of the Bethe-Salpeter equation with relativistic corrections to order  $1/m^2$ , or through the use of the Wilson loop technique [61].

the tensor interaction:

$$H_T = [(\vec{S}_1 \cdot \hat{r})(\vec{S}_2 \cdot \hat{r}) - (\vec{S}_1 \cdot \vec{S}_2)/3] \frac{1}{m^2 r} (V'_v - r V''_v) \quad (42)$$

and the spin-spin interaction:

$$H_{SS} = (\vec{S}_1 \cdot \vec{S}_2) \frac{2}{3m^2} \nabla^2 V_v \quad (43)$$

where  $\vec{L}, \vec{S}_1, \vec{S}_2$  are the orbital and spin angular momenta,  $V_v$  and  $V_s$  (with  $V = V_v + V_s$ ) transform as the time component of a four vector and as a Lorentz scalar, respectively,  $m$  is the quark mass, and primed quantities stand for the derivative  $d/dr$ .

The hyperfine splittings :

$$\Delta E_S = M(^3S_1) - M(^1S_0) \quad (44)$$

$$\Delta E_P = M_{cog}(^3P) - M(^1P_1) \quad (45)$$

are completely determined by the  $H_{SS}$  term<sup>6</sup>. Under the hypothesis that the vector part of the interaction is dominated by single gluon exchange the hyperfine splitting reduces to:

$$\Delta E_{S,P} \propto \langle \nabla^2 V_v(r) \rangle = \langle \frac{-4\alpha_s}{3} \nabla^2 \left( \frac{1}{r} \right) \rangle = \frac{-4\alpha_s}{3} \times |\psi(0)|^2 \quad (46)$$

where the expectation value is evaluated using the unperturbed wavefunction  $\psi(r)$ . Since  $\Delta E_{S,P}$  is proportional to the square of the wavefunction at the origin, then for single gluon exchange,  $L \neq 0$  singlet states would be degenerate with the triplet center-of-gravity. Therefore, the observation of such a hyperfine splitting signals deviations from the simple single gluon exchange hypothesis.

## 5.2 Charmonium Decay Rates

Decays of charmonium states that proceed through the annihilation of the quark-antiquark pair into  $e^+e^-$ ,  $\gamma\gamma$ , or multigluon final states, can be factored into two parts, one giving the probability of finding the quark-antiquark pair

---

<sup>6</sup>The quantity  $M_{cog}(^3P)$  in (45) has been defined in section 4.4.

at a distance where the annihilation can take place ( $\sim$  Compton wavelength of the quark  $\lambda_Q = 1/m$ ), and one describing the on-shell  $c\bar{c}$  hard process. The first factor can be expressed in terms of the wavefunctions for the  $c\bar{c}$  system, while the second factor is evaluated by using perturbative QCD.

In the Born approximation, a non relativistic derivation of the width for the decay of a singlet  $S$ -state of mass  $M$  to  $\gamma\gamma$  gives:

$$\Gamma(^1S_0 \rightarrow \gamma\gamma) = \frac{48\pi e_c^4 \alpha^2}{M^2} |\psi(0)|^2 \left(1 - \frac{3.4\alpha_s}{\pi}\right) \quad (47)$$

where  $e_c = 2/3$  is the  $c$ -quark charge in electron charge units and  $\alpha$  is the fine structure constant. The last factor includes first-order strong radiative corrections [47].

A generalization to hadronic processes such as:

$$^1S_0, ^3P_0, \text{ or } ^3P_2 \rightarrow gg; \quad ^3S_1, \text{ or } ^1P_1 \rightarrow ggg; \quad ^3P_1 \rightarrow gq\bar{q} \quad (48)$$

where the final state constituents fragment into light hadrons, gives for a state of principal quantum number  $n$  and orbital angular momentum  $l$ , the decay width:

$$\Gamma((\bar{c}c)_{nl} \rightarrow \text{light hadrons}) \propto \left| \frac{d^l}{dr^l} \psi_{nl}(0) \right|^2 F(\alpha_s) \quad (49)$$

where  $F(\alpha_s)$  is a power series in  $\alpha_s$ . For P-states, calculations along these lines lead to infrared divergences at order  $\alpha_s^3$ , that is to leading order for  $^3P_1$  and  $^1P_1$  states and to next-to-leading order for  $^3P_2$  and  $^3P_0$  states. It has been pointed out in a recent paper [54] that the appearance of infrared divergences is an indication of the breakdown of the factorization scheme adopted, and an alternative scheme has been suggested.

The hadronization process by which gluons transform into light-quark hadrons is not well understood. For the hadronization into a proton-antiproton pair, which also determines the cross section for  $(\bar{c}c)$  formation in the reverse reaction  $\bar{p}p \rightarrow (\bar{c}c)$ , estimates of the coupling of  $(\bar{c}c)$  states to  $\bar{p}p$  have been obtained in the framework of massless QCD [62]. The vector coupling of QCD requires that massless quarks have opposite helicities, a requirement that carries over to the annihilating  $p$  and  $\bar{p}$ . Thus only states of helicity  $\pm 1$  can be formed and the formation of  $J = 0$  states, such as the  $\eta_c$

and the  $\chi_{c0}$ , is forbidden. This rule is badly violated, which is not a surprise, since, in this energy regime, the mass of the proton is hardly a negligible quantity. An alternative model describes baryons as compound objects of quarks and diquark structures [63], but this model predicts for the partial width for  $\eta_c \rightarrow p\bar{p}$  a value much smaller than the one measured.

Radiative [64] or gluonic [65] transitions between two states of charmonium can be expressed in terms of multipoles of the electromagnetic or the gluonic field.

For  $P$  to  $S$  radiative decays:

$$(\bar{c}c)_{n,l} \rightarrow (\bar{c}c)_{n',l'} + \gamma \quad (50)$$

with  $n' = n$  and  $l' = l \pm 1$ , the electric dipole term dominates. In the limit of large wavelengths we have:

$$\Gamma_{fi} = \frac{4}{9} e_c^2 \alpha k^3 | \langle f | \vec{r} | i \rangle |^2 \quad (51)$$

where  $k = E_i - E_f$ , the differences between the energies of the initial and final state, and  $\vec{r} = \vec{r}_1 - \vec{r}_2$ . For charmonium the long wavelength limit ( $kr_B \ll 1$ ) is not satisfied, and corrections of order of ten percent in the above have to be applied for  $P$  to  $S$  transitions of states with equal  $n$ . The value of the overlap integral is sensitive to the choice of the potential used to derive the wavefunctions for the initial and final states and relativistic corrections can be substantial. For example in the decay  $1^1P_1 \rightarrow 1^1S_0 + \gamma$ , spin effects tend to shrink the wavefunction of the  $1^1S_0$  thereby reducing the overlap with the  $1^1P_1$  state. The experimental values for  $\Gamma(\chi_{c0,1,2} \rightarrow \psi + \gamma)$  are in good agreement with the predictions of recent calculations that include such relativistic corrections[54],[66], [67]. The same authors predict  $\Gamma(1^1P_1 \rightarrow \eta_c + \gamma) \approx 400keV$ .

The evaluation of transition rates for processes that involve the radiation of light quarks from the charmonium states, such as<sup>7</sup>:

$$(c\bar{c}) \rightarrow (c\bar{c})' + \pi^0 \quad ; \quad (c\bar{c}) \rightarrow (c\bar{c})' + \pi\pi \quad (52)$$

is more complicated. Perturbative QCD is not applicable in this case, where we have small energy difference and soft gluons are emitted, and one must

---

<sup>7</sup>The first decay mode shown does not conserve Isospin

resort to phenomenological models. There are two conflicting predictions [68],[69] for the relative decay rates of the  $^1P_1$  to  $\psi\pi^0$  and to  $\psi\pi\pi$ , and the results of E760 will help in clarifying this situation.

## 5.3 Determination of $\alpha_s$ from Charmonium Data

### 5.3.1 Annihilations

The widths for charmonium decays through the annihilation process depend on the charmed quark mass  $m$ , the wavefunction of the system at the origin  $\psi(0)$ , and the strong coupling constant  $\alpha_s$ . Ratios of rates for two annihilation processes of the same state are largely independent of  $m$  and  $\psi(0)$ . In principle it should be possible to extract from such ratios a value for  $\alpha_s$ . However, only calculations to next to leading order in the perturbation series are available, yielding results which are not unique but depend on the precise definition of the coupling constant (the renormalization scheme) and on the choice of the mass  $\mu$  (the renormalization scale) where  $\alpha_s$  is defined<sup>8</sup>. These unphysical ambiguities will disappear in calculations made to all orders. For some processes the next-to-leading order term is comparable in magnitude to the leading order one, and the convergence of the perturbation series is in question. Without further probing this treacherous subject, we will compare the quoted experimental results to the expressions given in [47] where  $\mu = m = 1.5 \text{ GeV}$  is chosen<sup>9</sup>. For the  $\eta_c$ :

$$\frac{\Gamma(\eta_c \rightarrow \gamma\gamma)}{\Gamma(\eta_c \rightarrow \text{gluons})} = \frac{8\alpha_s^2}{9\alpha_s^2} \frac{1 - 3.4\alpha_s/\pi}{1 + 4.8\alpha_s/\pi} \sim B(\eta_c \rightarrow \gamma\gamma) = (3.0 \pm 1.2) \times 10^{-4} \quad (53)$$

from which  $\alpha_s(\mu = 1.5 \text{ GeV}) = 0.40_{-0.07}^{+0.11}$  to leading order or  $\alpha_s(\mu = 1.5 \text{ GeV}) = 0.28_{-0.04}^{+0.06}$  to next to leading order.

One would be tempted to apply the same method to extract  $\alpha_s$  from the ratio

$$\frac{\Gamma(\chi_2 \rightarrow \gamma\gamma)}{\Gamma(\chi_2 \rightarrow \text{gluons})} = (1.9 \pm 0.6) \times 10^{-4} \quad (54)$$

<sup>8</sup>There are suggestions in the literature as to how one chooses the renormalization scale in a way that minimizes these ambiguities [70].

<sup>9</sup>Note that the  $\alpha_s$  used in the discussion of this section is the one defined in the modified minimal subtraction scheme, i.e.  $\alpha_{\overline{MS}}$ .

obtaining  $\alpha_s(\mu = 1.5 \text{ GeV}) = 0.50_{-0.07}^{+0.10}$  to leading order and  $\alpha_s(\mu = 1.5 \text{ GeV}) = 0.36 \pm 0.04$  to next-to-leading order. However, as we have seen, the presence of infrared divergences in the next-to-leading order corrections casts doubts on the validity of this derivation.

### 5.3.2 The Hyperfine Splittings

The values for the hyperfine splitting are :

$$\Delta E_S = M(J/\psi) - M(\eta_c) = 109.4_{-2.8}^{+3.0} \text{ MeV} \quad (55)$$

$$\Delta E_P = M_{cog} - M(h_c) = -0.93 \pm 0.28 \text{ MeV} \quad (56)$$

where we have used the masses for the  $J/\psi$ ,  $\eta_c$ ,  $\chi_{c1}$ ,  $\chi_{c2}$ , and  $h_c$  obtained by E760, and the  $\chi_{c0}$  mass from Ref.[20] ( $3415.1 \pm 1.0 \text{ MeV}$ ). With this choice we have  $M_{cog} = 3525.27 \pm 0.12 \text{ MeV}$ .

The fact that  $\Delta E_P$  is negative excludes many of the mechanisms proposed to shift the  $h_c$  mass from  $M_{cog}$  [72]. An approach that predicts the correct sign and magnitude for this shift is one[73] that evaluates the hyperfine splitting to one loop in perturbative QCD. In a recent version of this calculation[74]  $\Delta E_P$  was given in a form that does not depend on the mass scale ( $\mu$ ) and the renormalization scheme, but depends only on the value of the coupling constant  $\alpha_s$  and of the mass of the constituent quark  $m$ . From the measured value of  $\Delta E_P$  one finds that  $\alpha_s = 0.28 \pm 0.02$  for  $m = 1.2 \text{ GeV}$  or  $\alpha_s = 0.33 \pm 0.02$  for  $m = 1.8 \text{ GeV}$ . In contrast the hyperfine splitting of the  $S$  states as given in Ref.[74] is not independent of the renormalization scale. Choosing  $\mu = m$  one finds from the comparison with the experimental result values of  $\alpha_s$  vs  $m$  consistent with the result obtained for the  $P$  states. With this choice for the mass scale the contribution of the second order corrections is much smaller than the leading (first) order one, as one would expect for a reliable application of PQCD.

### 5.3.3 Discussion

The derivation of  $\alpha_s$  from charmonium data presents several problems. If one uses the ratio of the measured annihilation rates of the  $\eta_c$  into  $\gamma\gamma$  and into light hadrons, one is faced with the large uncertainties in the measured value of  $B(\eta_c \rightarrow \gamma\gamma)$ , and, more important, is limited by the poor understanding of the convergence of the perturbation series and of the ambiguities

introduced by the choice of a mass-scale. The estimation of  $\alpha_s$  from the hyperfine splitting of P-states is more robust, since it is based on a more precise measurement and is less affected by such theoretical uncertainties. However the value derived for  $\alpha_s$  in this fashion still depends on the value of the mass of the constituent quark, a quantity rather poorly defined.

The determination of  $\alpha_s$  using the  $1S - 1P$  mass splitting as an input to lattice gauge calculations is one of the most reliable methods at this time. As the methods used in these calculations improve, it is probable that this technique will yield the best measurement for  $\alpha_s$ . The value of  $\alpha_s(5\text{GeV}) = 0.174 \pm 0.012$  of Ref.[56] extrapolated to our energy scale gives  $\alpha_s(1.2\text{GeV}) = 0.279^{+0.038}_{-0.028}$  and  $\alpha_s(1.5\text{GeV}) = 0.253^{+0.032}_{-0.022}$ .

## 6 OUTLOOK

It has been almost 20 years since charmonium swept the field of particle physics, and still the study of this system remains a vital and worthwhile endeavor. The high precision measurements that have been achieved through the study of charmonium produced in proton-antiproton annihilations, together with the opportunity for discovering states not accessible in electron-positron annihilations are the major reasons for the vitality of this field. It is almost surprising that with the observation of the  $h_c(1^1P_1)$  our qualitative knowledge of the charmonium spectrum is more complete than our knowledge of the positronium spectrum!

Just as positronium has been one of the proving grounds of QED, charmonium has provided some of the more stringent tests of QCD. The new precise measurements from R704 and E760 make comparison with theory even more challenging. We look forward to the continuation of this series of experiments at Fermilab[75] where even more accurate measurements of the  $\chi_{c0}, h_c, \eta_c, \eta'_c$  states, as well as the potential for observing as yet undetected states of charmonium (such as the  $^3D_2, ^1D_2$ ), will extend the range of tests of QCD.

## References

- [1] Gross D, Wilczek F. *Phys. Rev. Lett.* 30:1343 (1973); Politzer HD. *Phys.*

- Rev. Lett.* 30:1346 (1973).
- [2] Aubert JJ et al. *Phys. Rev. Lett.* 33:1404 (1974); Augustin JE et al. *Phys. Rev. Lett.* 33:1406 (1974).
  - [3] For a review of the early  $e^+e^-$  experiments, see Feldman GJ, Perl ML. *Phys. Rep. C* 19:233 (1975); Feldman GJ, Perl ML. *Phys. Rep. C* 33:285 (1977).
  - [4] Eichten E et al. *Phys. Rev. Lett.* 34:369 (1975).
  - [5] The quarkonia bibliography is immense, a convenient collection of many of the more significant theoretical papers is: *Quarkonia, Current Physics – Sources and Comments; Vol. 9*, ed. W. Buchmüller. Amsterdam: North-Holland (1992).
  - [6] Kronfeld AS, Mackenzie PB. *Ann. Rev. Nucl. Part. Sci.* 43:793 (1993); Mackenzie PB. 1993. In *Lattice 92, Int. Symp. on Lattice Field Theory*, ed. J. Smit and P. Van Baal. *Nucl. Phys. B (Proc. Suppl.)* 30:35 (1993); Lepage GP. In *Lattice 91, Int. Symp. on Lattice Field Theory*, ed. M. Fukugita et al. *Nucl. Phys. B (Proc. Suppl.)* 26:45 (1992).
  - [7] Fitch VL, private communication. See also ref. 18 in our ref 4.
  - [8] Cole FT, Mills FE. *Ann. Rev. Nucl. Part. Sci.* 31:295 (1981); Möhl D et al. *Phys. Rep. C* 58:73 (1980).
  - [9] Arnison G et al. *Phys. Lett. B* 122:103 (1983); Arnison G et al. *Phys. Lett. B* 126:398 (1983).
  - [10] Dalpiaz P. In *Proceedings of the first LEAR workshop*, ed. H. Poth, Karlsruhe: Kernforschungszentrum (1979).
  - [11] Baglin C et al. *CERN Proposal CERN/ISRC/80-14*, unpublished (1980).
  - [12] Bharadwaj V et al. *Fermilab Proposal P760*, unpublished (1985).
  - [13] Baglin C et al. *Nucl. Phys. B* 286:592 (1987).

- [14] Henrichsen KN, De Jonge MJ. Report CERN/ISR/RF/MA 74-21 (1974); Montague BW. In *Theoretical Aspects of the Behaviour of Beams in Accelerators and Storage Rings* ed. M.H. Blewett, CERN report 77-13, Geneva: CERN, p. 63 (1977).
- [15] Macrí M. In *Antiprotons for colliding beam facilities: Proceedings of the 1983 CERN Accelerator School*, ed. P. Bryant and S. Newman (CERN 84-15), p. 469, (1984).
- [16] Chattopadhyay S. In *AIP Conf. Proc. 127: Physics of High Energy Accelerators*, ed. M. Month, P. F. Dahl, M. Dienes, New York: AIP (1985)
- [17] Brom J-M. *Formation des Etats Charmonium dans le Canal Direct d'Annihilation  $p\bar{p}$  et Description d'une Methode Experimentale Nouvelle. Reactions Exclusives  $p\bar{p} \rightarrow e^+e^-$* . PhD Thesis. CRN, Strasbourg. (1985).
- [18] Peoples, Jr. J. In *Proceedings of the Workshop on the Design of a Low Energy Antimatter Facility*, ed. D. Cline, p. 144, Singapore: World Scientific, (1986).
- [19] Tollestrup AV, Dugan G. In *AIP Conf. Proc. 105: Physics of High Energy Accelerators*, ed. M. Month, New York: AIP (1983); Petter J et al. In *Proceedings of the 1989 IEEE Particle Accelerator Conference*, Vol. 1, 648 (1989).
- [20] Hikasa K et al. (Particle Data Group). *Phys. Rev. D* 45:S1 (1992); erratum 46:5210 (1992).
- [21] Rosen J, private communication.
- [22] Armstrong TA et al. *Phys. Rev. D* 47:772 (1993).
- [23] Due to S. Y. Hsueh, private communication.
- [24] Kennedy DC. *Phys. Rev. D* 46:461 (1992).
- [25] Armstrong TA et al. *Phys. Rev. Lett.* 70:1212 (1993).
- [26] Baglin C et al. *Phys. Lett. B* 163:400 (1985).

- [27] Lepage GP, Brodsky SJ. *Phys. Rev. Lett.* 43:545 (1979); Lepage GP, Brodsky SJ. *Phys. Rev. D* 22:2157 (1980).
- [28] Feldman GJ. In *Proc. 19th Int. Conf. on High Energy Physics*, ed. S. Homma, M. Kawaguchi, M. Miyazawa. Tokyo: Physical Soc. of Japan, p. 777 (1978).
- [29] Baglin C et al. *Phys. Lett. B* 172:455 (1986).
- [30] Oreglia MJ. *A Study of the Reactions  $\psi' \rightarrow \gamma\gamma\psi$* . Ph. D. Thesis. Stanford University, Stanford, SLAC report 236 (1980).
- [31] Armstrong TA et al. *Nucl. Phys. B* 373:35 (1992).
- [32] Armstrong TA et al. *Phys. Rev. Lett.* 68:1468 (1992).
- [33] Armstrong TA et al. *Phys. Rev. D* 48:3037 (1993).
- [34] Baglin C et al. *Phys. Lett. B* 195:85 (1987).
- [35] Oreglia M et al. *Phys. Rev. D* 25:2259 (1982).
- [36] Armstrong TA et al. *Phys. Rev. Lett.* 69:2337 (1992).
- [37] Baglin C et al. *Phys. Lett. B* 171:135 (1986).
- [38] Gaillard MK et al. *Phys. Lett. B* 110:489 (1982).
- [39] Armstrong TA et al. FERMILAB-Pub-94/042-E, (1994) Batavia: Fermilab. To be submitted to *Phys. Rev. D*.
- [40] Baglin C et al. *Phys. Lett. B* 187:191 (1987).
- [41] Chen W-Y et al. *Phys. Lett. B* 243:169 (1990).
- [42] Aihara H et al. *Phys. Rev. Lett.* 60:2355 (1988).
- [43] Berger Ch. et al. *Phys. Lett. B* 167:120 (1986).
- [44] Braunschweig C et al. *Z. Phys. C* 41:533 (1989).

- [45] Križan P et al. In *Proc. of the 1991 Joint Int. Lepton Photon Symposium and Europhysics Conf. on High Energy Physics* ed. S. Hegarty, K. Potter, and E. Quercigh. Singapore: World Scientific, p.92 (1992)
- [46] Adriani O et al. Measurement of  $\eta_c$  Production in Untagged Two-Photon Collisions at LEP. CERN PPE 93-173 (submitted for publication in Phys.Lett.B)
- [47] Kwong W et al. *Phys. Rev. D* 37:3210 (1988).
- [48] Ackleh ES, Barnes T. *Phys. Rev. D* 45:232 (1992).
- [49] Barnes T. In *IXth International Workshop on Photon-Photon Collisions* ed. D.O. Caldwell, H.P. Paar. Singapore: World Scientific, p.263 (1992).
- [50] Armstrong TA et al. *Phys. Rev. Lett.* 70:2988 (1993).
- [51] Uehara S et al. *Phys. Lett. B* 266:188 (1991).
- [52] Lee RA. *Radiative Decays of the  $\psi'$  to All-Photon Final States*. Ph.D. Thesis. Stanford University, Stanford, SLAC report 282 (1985).
- [53] Yamada S. In *Proc. of the 1977 Int. Symposium on Lepton and Photon Interactions at High Energy* ed. F. Gutbrod, Hamburg: DESY, p.69 (1977).
- [54] Bodwin GT, Braaten E, Lepage GP. *Phys. Rev. D* 46:1914 (1992).
- [55] Edwards C et al. *Phys. Rev. Lett.* 48:70 (1982).
- [56] El-Khadra AX et al. *Phys. Rev. Lett.* 69:729 (1992).
- [57] Lucha W, Schöberl FF, Gromes D. *Phys. Rep. C* 200:127 (1991).
- [58] Grosse H. *Phys. Lett. B* 68:343 (1977); Martin A., CERN-TH.6933/93 (1993) to appear in *30th Course of the Int. School of Subnuclear Physics, Erice, 1993*.
- [59] Michael C. *Phys. Rev. Lett.* 56:1219 (1986).
- [60] Gromes D. *Z. Phys. C* 11:147 (1981); erratum 14:94 (1982).

- [61] Eichten E, Feinberg F. *Phys. Rev. D* 23:2724 (1981).
- [62] Brodsky SJ, Lepage GP. *Phys. Rev. D* 24:2848 (1981); Andrikopoulou A. *Z.Phys. C* 22:63 (1984).
- [63] Anselmino M et al. *Phys. Rev. D* 38:3516 (1988).
- [64] Novikov VA et al. *Phys. Rep. C* 41:1 (1978).
- [65] Gottfried K., *Phys. Rev. Lett.* 40:598 (1978); Yan T. *Phys. Rev. D* 22:1652 (1980).
- [66] McClary R, Byers N. *Phys. Rev. D* 28:1692 (1983).
- [67] Chao K et al. *Phys. Lett. B* 301:282 (1993).
- [68] Voloshin MB. *Sov. J. Nucl. Phys.* 43:1011 (1986).
- [69] Kuang Y et al. *Phys. Rev. D* 37:1210 (1988).
- [70] Brodsky SJ, Lepage GP, Mackenzie PB. *Phys. Rev. D* 28:228 (1983).
- [71] Olsson MG, Martin AD, Peacock AW. *Phys. Rev. D* 31:81 (1985).
- [72] Lichtenberg DB, Potting R. *Phys. Rev. D* 46:2150 (1992); see this paper for earlier references on evaluations of  $\Delta E_P$ .
- [73] Gupta SN, Radford SF, Repko WW. *Phys. Rev. D* 34:201 (1986); Pantaleone J, Tye S-HH, Ng YJ. *Phys. Rev. D* 33:777 (1986).
- [74] Halzen F et al. *Phys. Rev. D* 47:3013 (1993).
- [75] Cester R et al. *Fermilab proposal P835*, unpublished (1990); Armstrong TA et al. *Fermilab proposal P835(revised)*, unpublished (1992).

## Figure Captions

Figure 1 : Schematic of the R704 target system[13] : Chambers 1,2,3 are the production stage and 4,5 the sink stage. The gas jet intersects the antiproton beam at  $90^\circ$ .

Figure 2 : Top view of the R704 two-arm detector and part of the target system[13].

Figure 3 : E760 equipment layout[31].

Figure 4 : Invariant mass distribution of  $e^+e^-$  pairs for events taken at the  $\psi'$  formation energy (open area) and off-resonance (shaded area), normalized to equal luminosities[22].

Figure 5 : Events per unit luminosity for the energy scan at the  $\psi'$ . The dashed line is the center of mass energy resolution[32].

Figure 6 : Schematic for the sequence of the double scan.

Figure 7 :  $J/\psi$  and  $\psi'$  double scans. The horizontal axis is the invariant mass of the *central* orbit. The lines are theoretical excitation curves using the best fit parameters[22].

Figure 8 : Variation of  $q^4|G_M|/\mu_p$  with  $-q^2$ . The dashed curve shows a perturbative QCD fit ( $q^4|G_M| \propto \alpha_s^2(q^2) \propto 1/\ln(q^2/\Lambda^2)$ , with  $\Lambda = 0.2\text{GeV}$ ) for  $-q^2 \geq 5(\text{GeV}/c)^2$ . From Ref.[25].

Figure 9 : Comparison of the distribution of  $\chi_{c1}$  and  $\chi_{c2}$  events vs center of mass energy from (a) the Crystal Ball experiment[30], with (b) the excitation curves for  $\chi_{c1}$  and  $\chi_{c2}$  as measured by the R704 collaboration[29].

Figure 10 : Excitation curves for  $\chi_{c1}$  and  $\chi_{c2}$  measured by the E760 collaboration[31]. The dotted curves show the resolution in the center of mass energy.

Figure 11 : Invariant mass distribution of  $e^+e^-$  pairs for events collected during the  $1^1P_1$  search[36].

Figure 12 : Cross section vs center-of-mass energy for  $\bar{p}p \rightarrow \psi + \pi^0$  measured by the E760 collaboration[36], and cross section vs center-of-mass energy for  $\bar{p}p \rightarrow \psi + \dots$  measured by the R704 collaboration[37]. Acceptance and reconstruction efficiencies have been corrected for to make the two plots directly comparable.

Figure 13 : Measured[39] cross section for  $\bar{p}p \rightarrow \gamma\gamma$  vs center-of-mass energy at the  $\eta_c$ . The events were selected with  $|\cos(\theta_\gamma^*)| \leq 0.25$  on the  $\gamma\bar{p}$  angle in the center-of-mass system, to optimize the signal-to-background ratio.

Figure 14 : Measured[50],[39] cross section for  $\bar{p}p \rightarrow \gamma\gamma$  vs center-of-mass energy over an energy range where  $1P$  states, and  $2S$  states are formed. These events were selected cutting at  $|\cos(\theta_\gamma^*)| \leq 0.4$ .

Figure 15 : Search for the  $\eta'_c$  : upper limits[39] on the product  $B_{in} \times B_{out} \times 10^8$ .

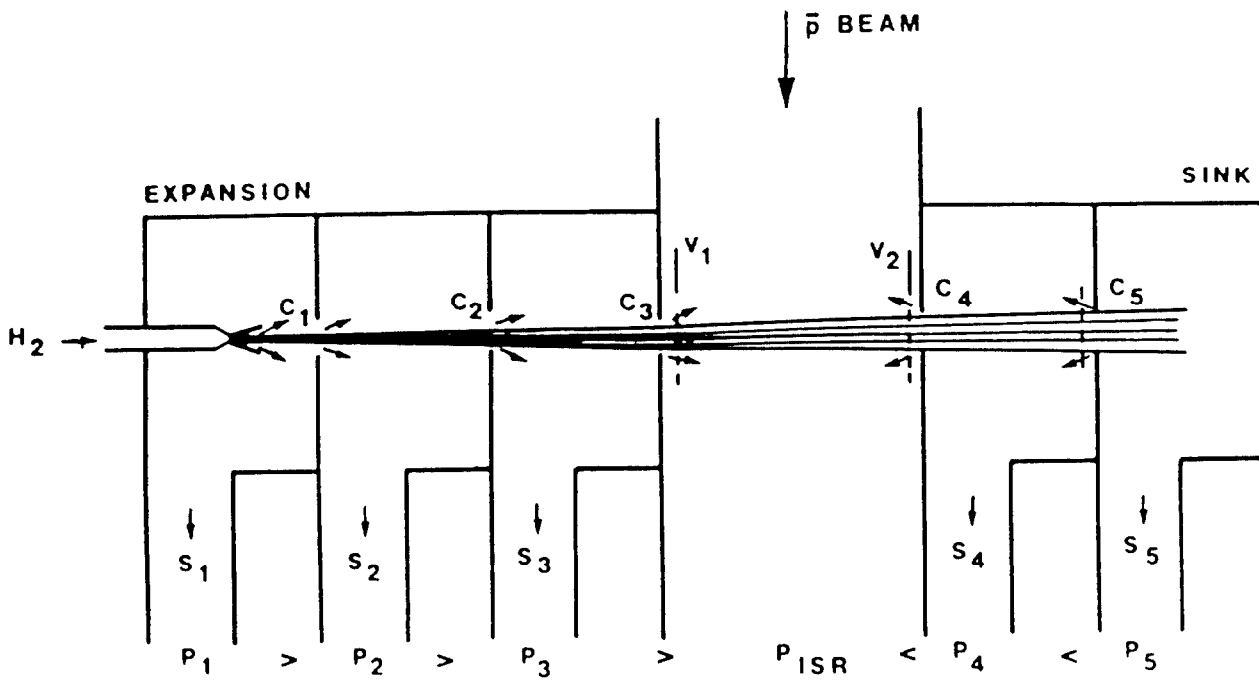


Figure 1 : Schematic of the R704 target system[13] : Chambers 1,2,3 are the production stage and 4,5 the sink stage. The gas jet intersects the antiproton beam at  $90^\circ$ .

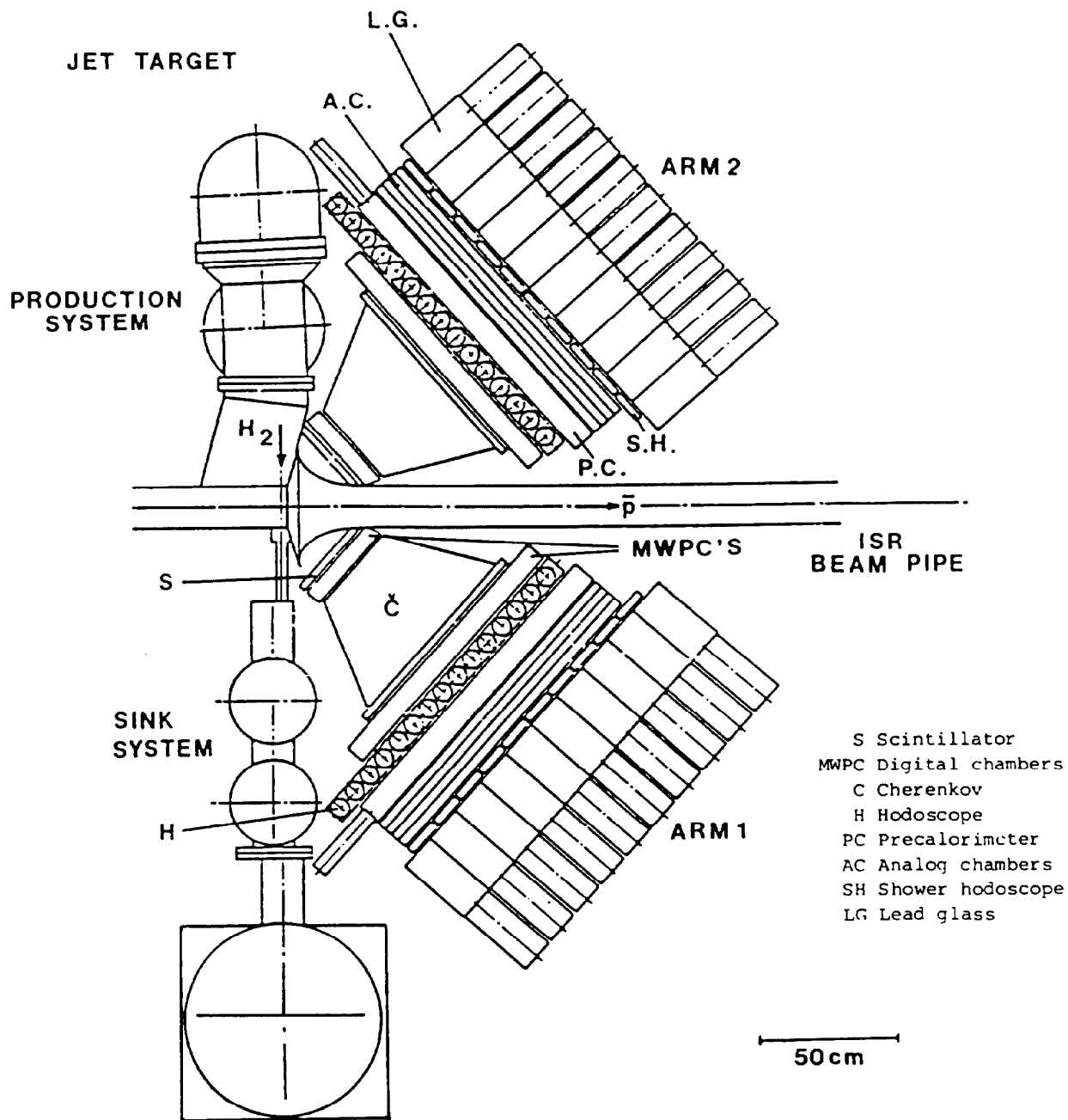


Figure 2 : Top view of the R704 two-arm detector and part of the target system[13].

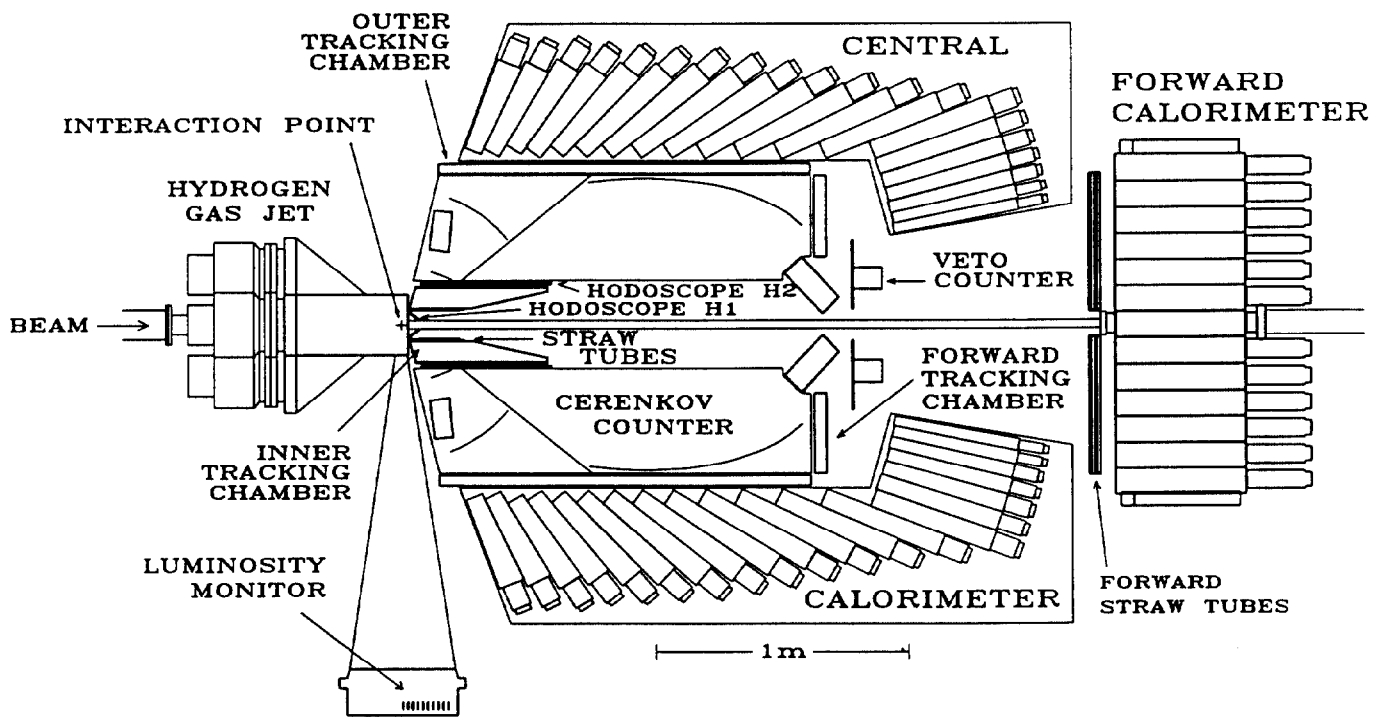


Figure 3 : E760 equipment layout[31].

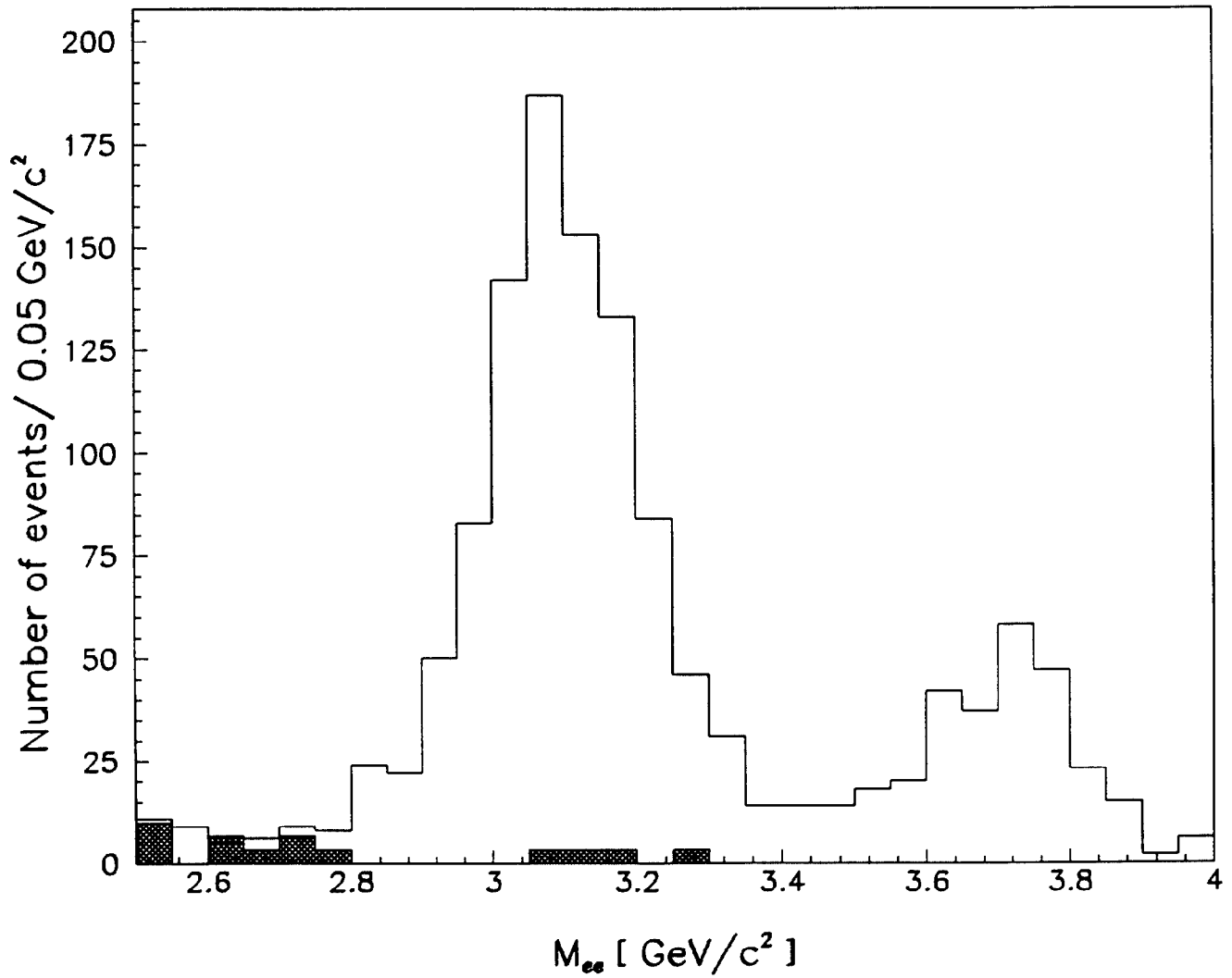


Figure 4 : Invariant mass distribution of  $e^+e^-$  pairs for events taken at the  $\psi'$  formation energy (open area) and off-resonance (shaded area), normalized to equal luminosities[22].

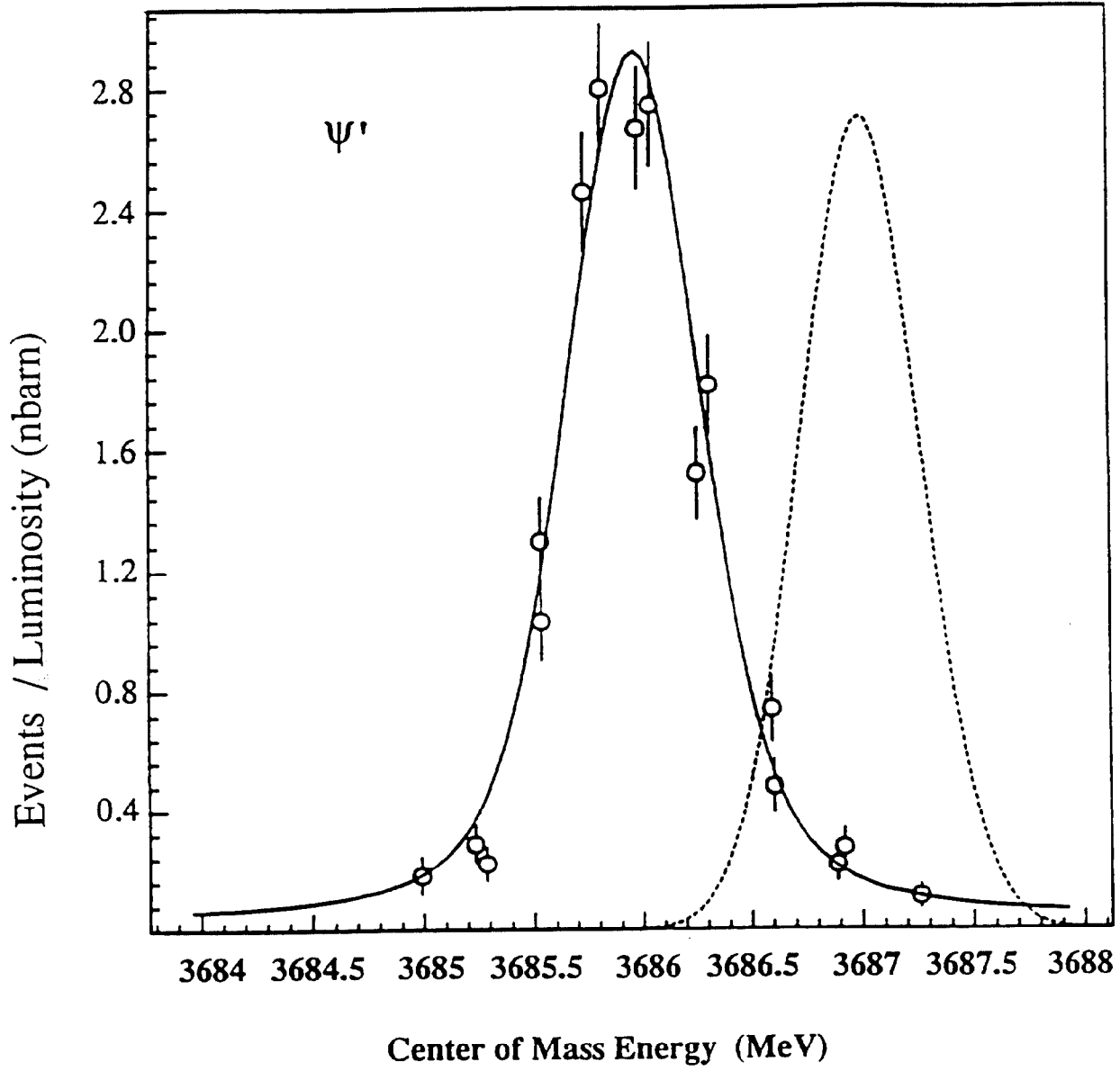


Figure 5 : Events per unit luminosity for the energy scan at the  $\psi'$ . The dashed line is the center of mass energy resolution[32].

# Schematic for double scan

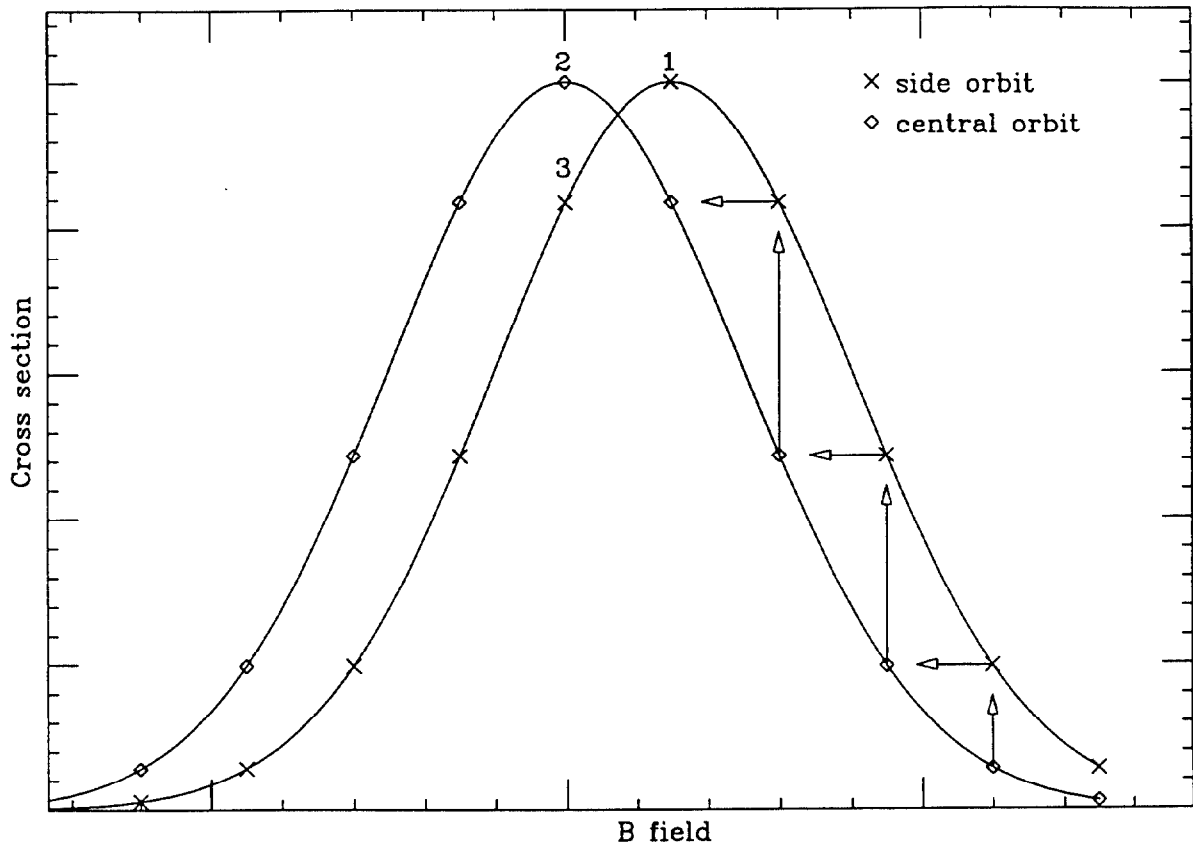


Figure 6 : Schematic for the sequence of the double scan.

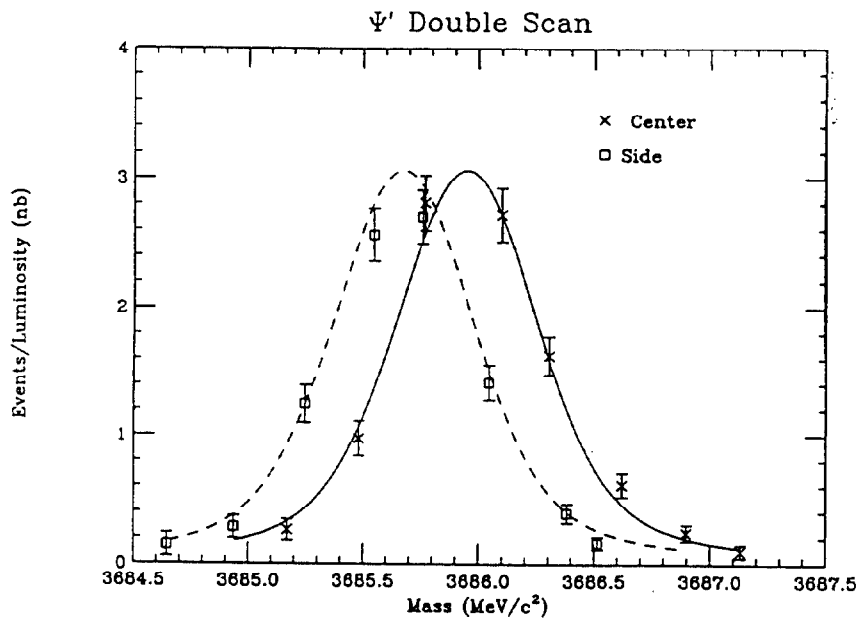
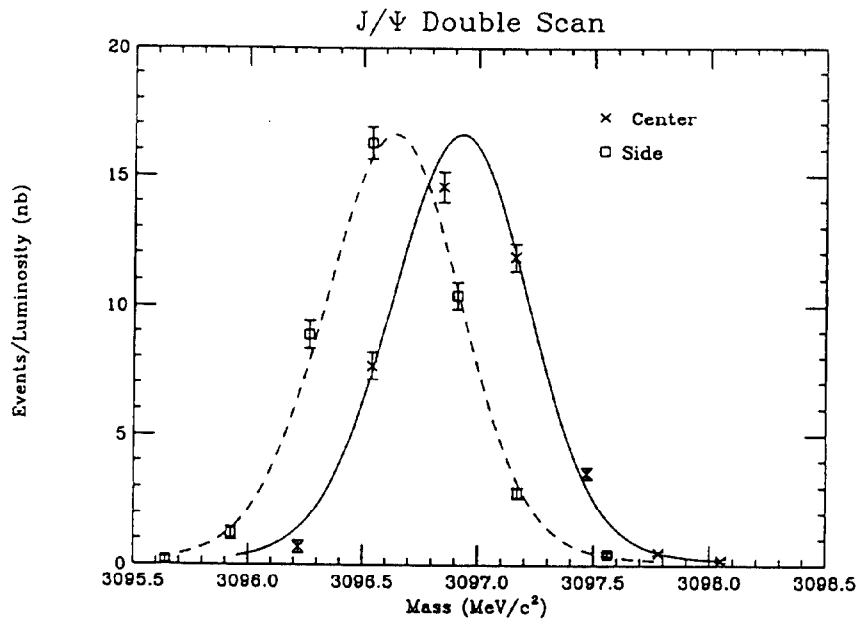


Figure 7 :  $J/\psi$  and  $\psi'$  double scans. The horizontal axis is the invariant mass of the *central* orbit. The lines are theoretical excitation curves using the best fit parameters[22].

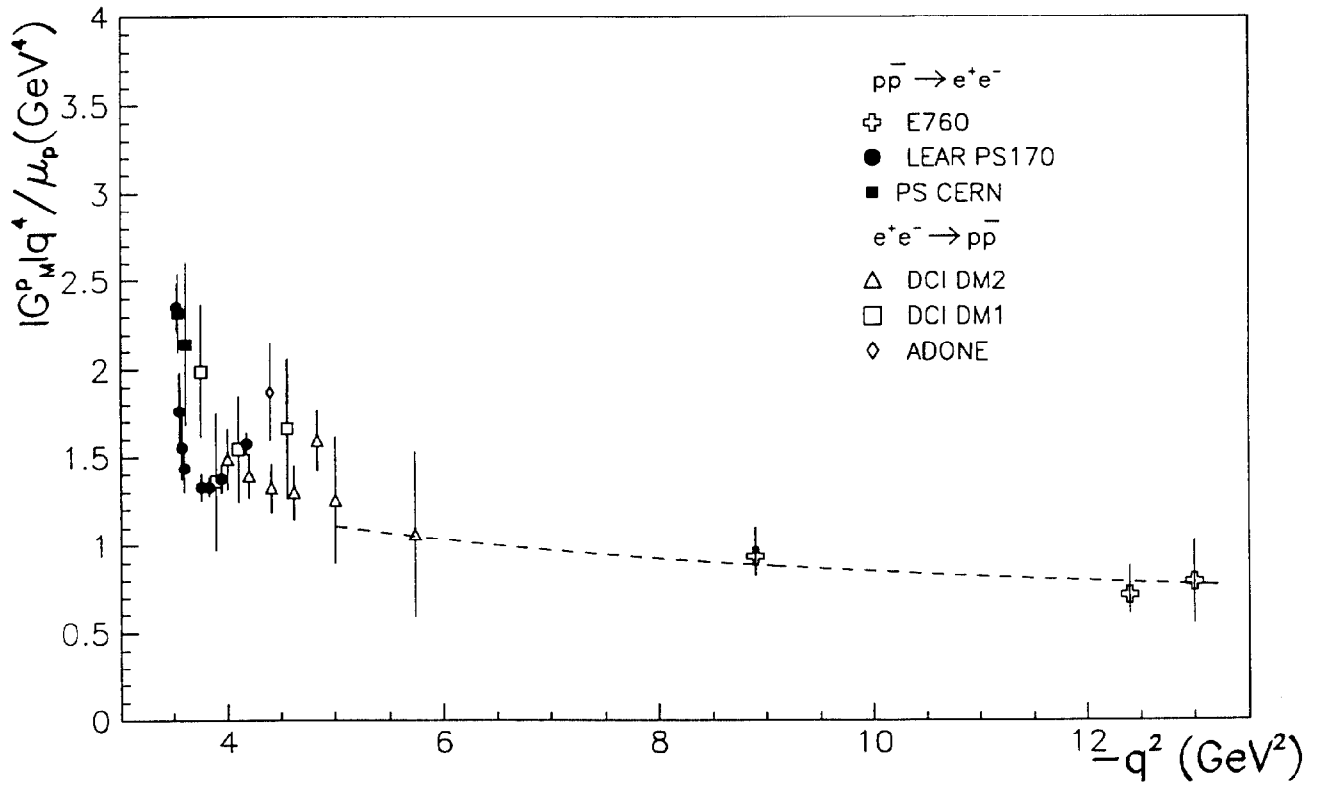


Figure 8 : Variation of  $q^4|G_M|/\mu_p$  with  $-q^2$ . The dashed curve shows a perturbative QCD fit ( $q^4|G_M| \propto \alpha_s^2(q^2) \propto 1/\ln(q^2/\Lambda^2)$ , with  $\Lambda = 0.2\text{GeV}$ ) for  $-q^2 \geq 5(\text{GeV}/c)^2$ . From Ref.[25].

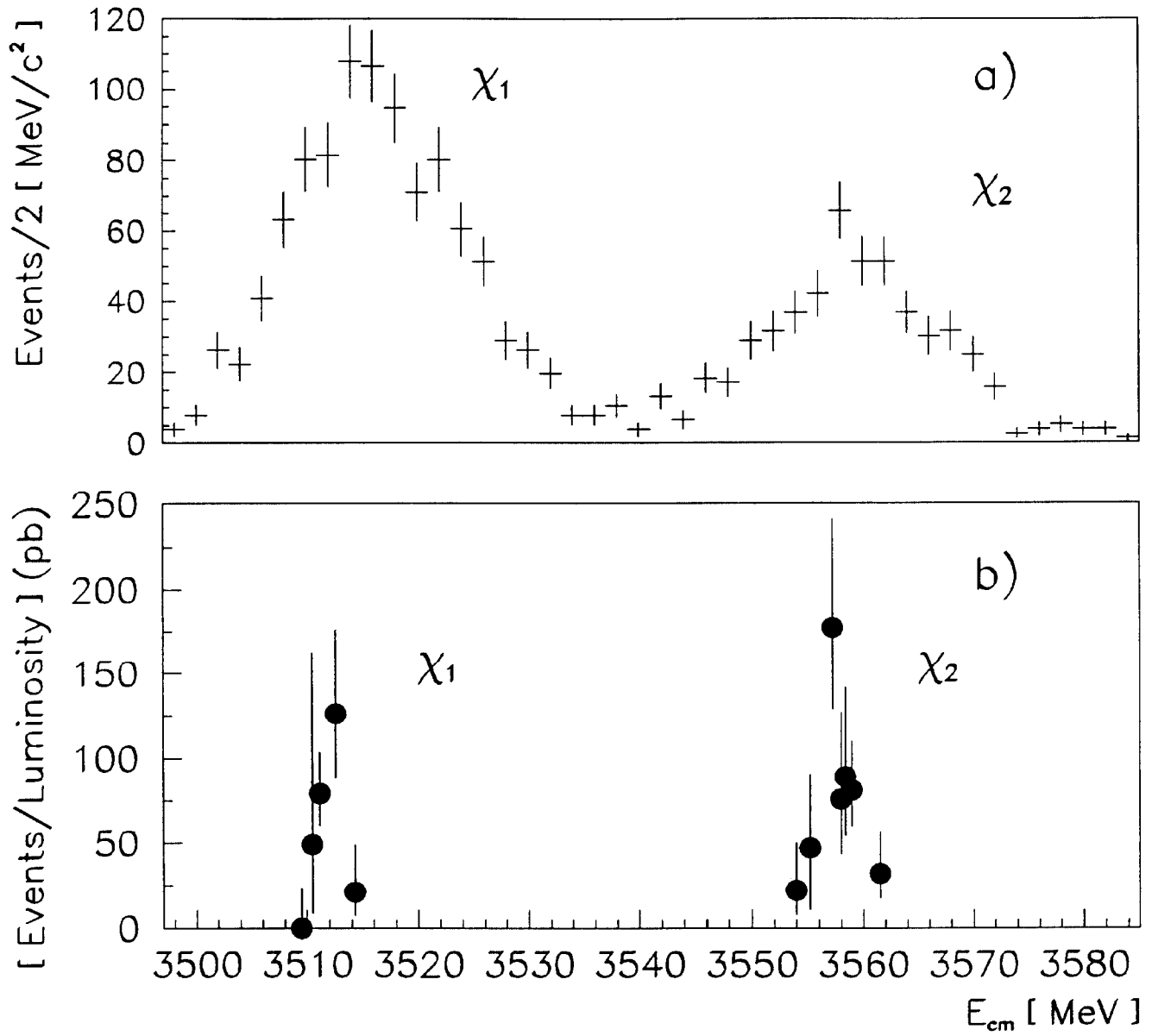


Figure 9 : Comparison of the distribution of  $\chi_{c1}$  and  $\chi_{c2}$  events vs center of mass energy from (a) the Crystal Ball experiment[30], with (b) the excitation curves for  $\chi_{c1}$  and  $\chi_{c2}$  as measured by the R704 collaboration[29].

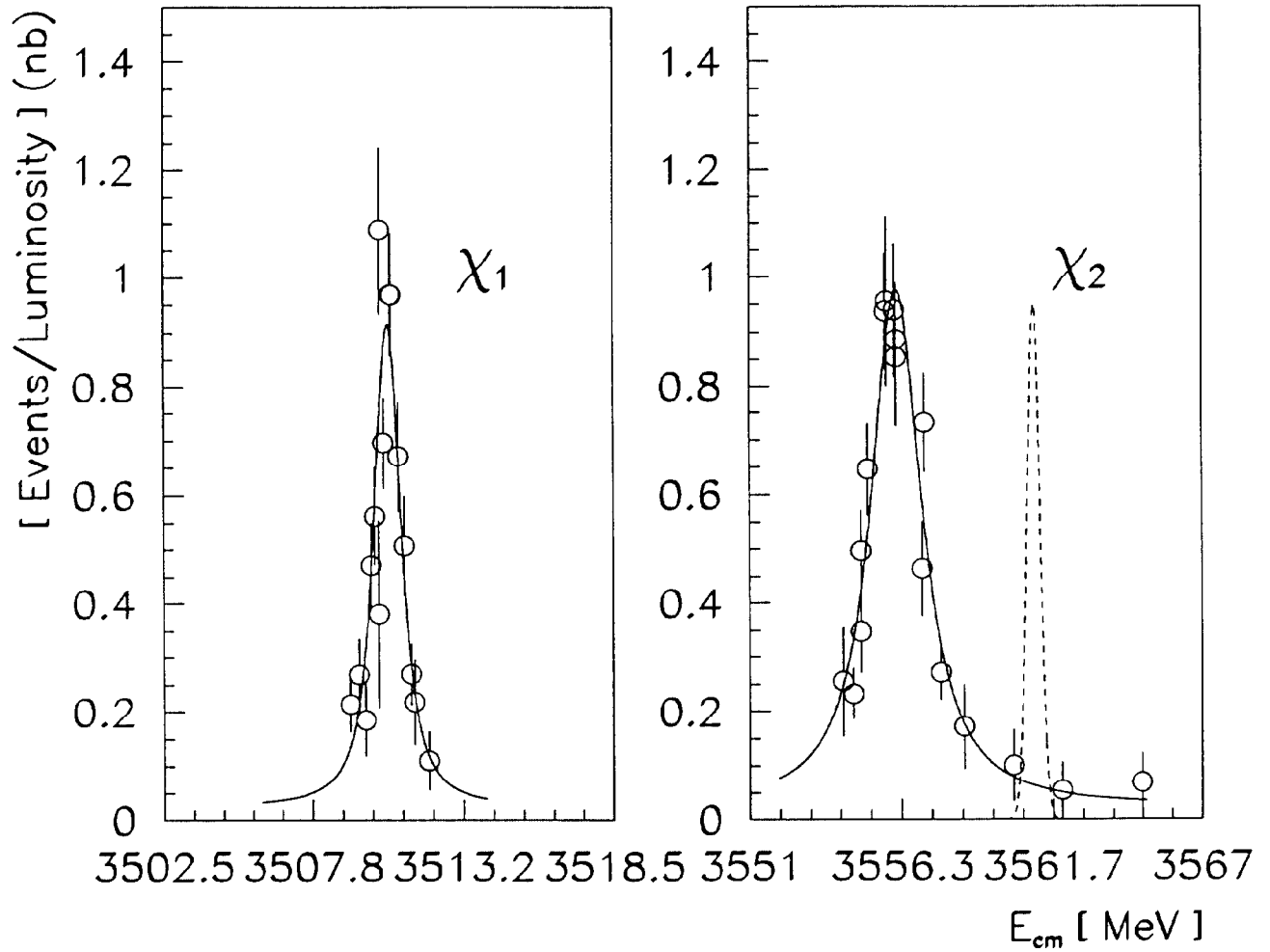


Figure 10 : Excitation curves for  $\chi_{c1}$  and  $\chi_{c2}$  measured by the E760 collaboration[31]. The dotted curves show the resolution in the center of mass energy.

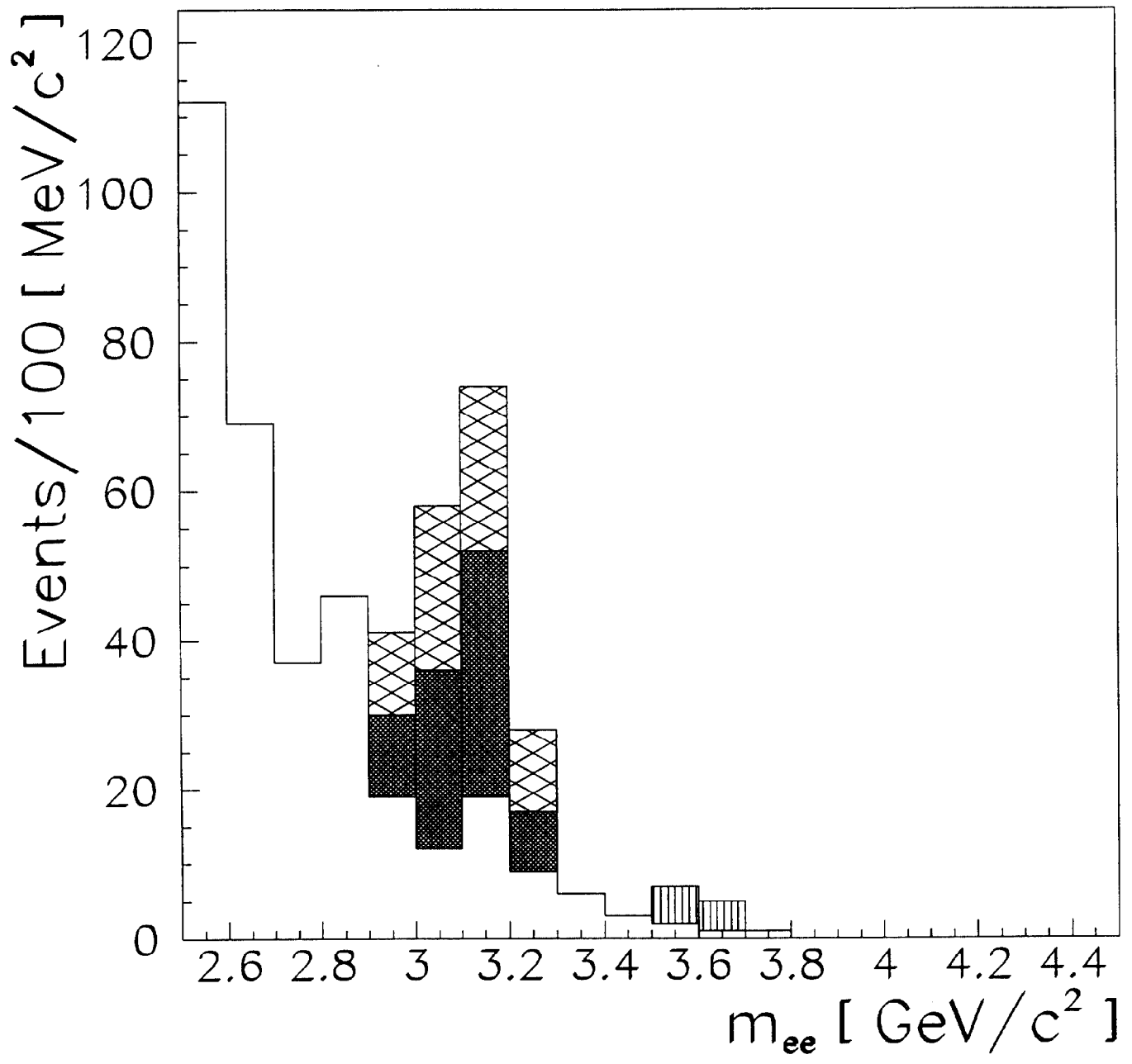


Figure 11 : Invariant mass distribution of  $e^+e^-$  pairs for events collected during the  $1^1P_1$  search[36].

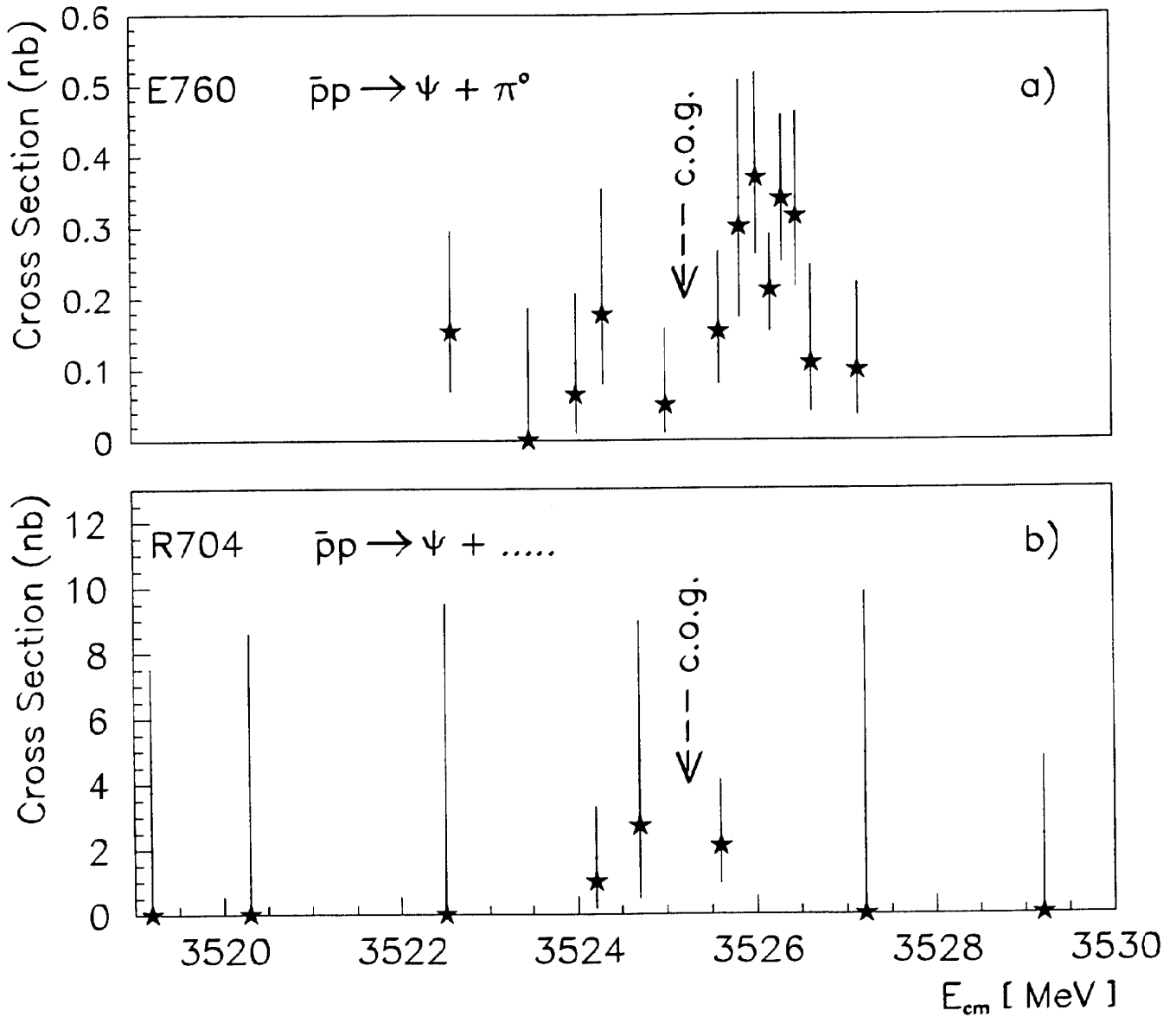


Figure 12 : Cross section vs center-of-mass energy for  $\bar{p}p \rightarrow \psi + \pi^0$  measured by the E760 collaboration[36], and cross section vs center-of-mass energy for  $\bar{p}p \rightarrow \psi + \dots$  measured by the R704 collaboration[37]. Acceptance and reconstruction efficiencies have been corrected for to make the two plots directly comparable.

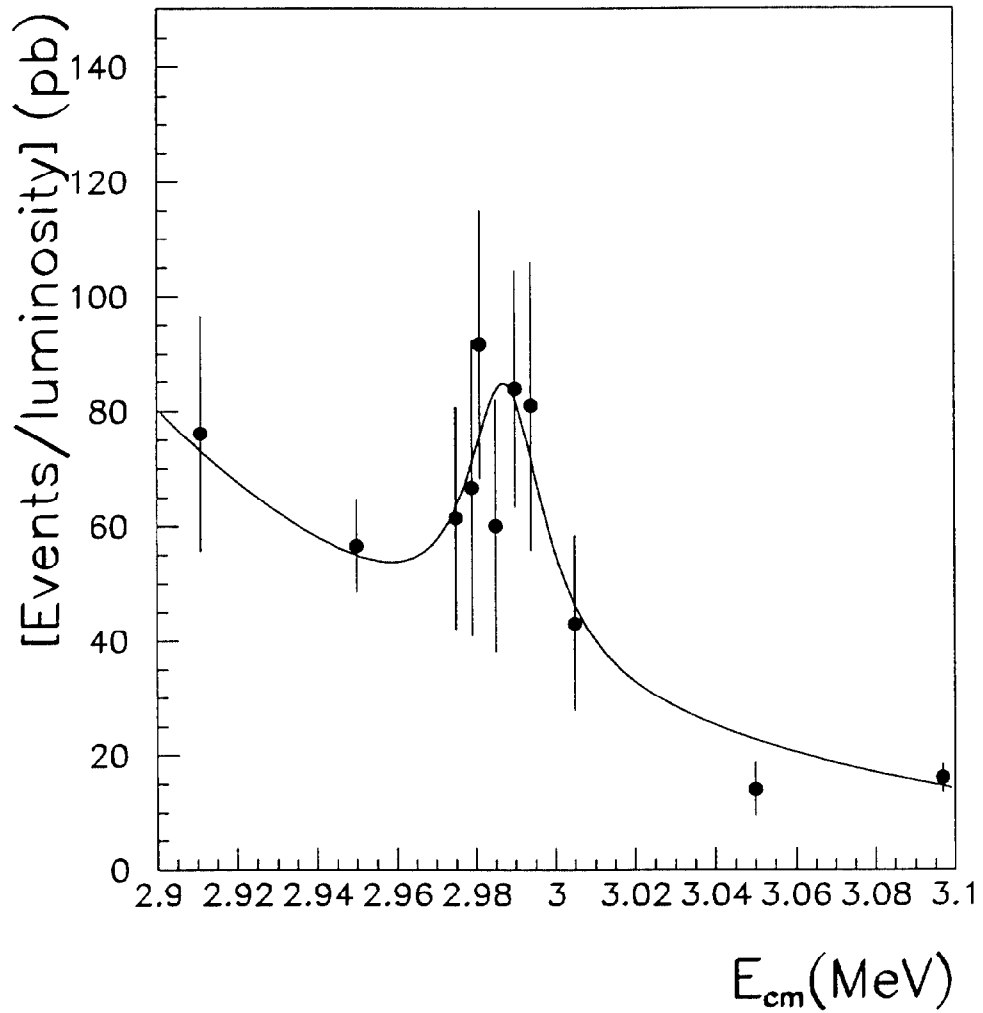


Figure 13 : Measured[39] cross section for  $\bar{p}p \rightarrow \gamma\gamma$  vs center-of-mass energy at the  $\eta_c$ . The events were selected with  $|\cos(\theta_\gamma^*)| \leq 0.25$  on the  $\gamma\bar{p}$  angle in the center-of-mass system, to optimize the signal-to-background ratio.

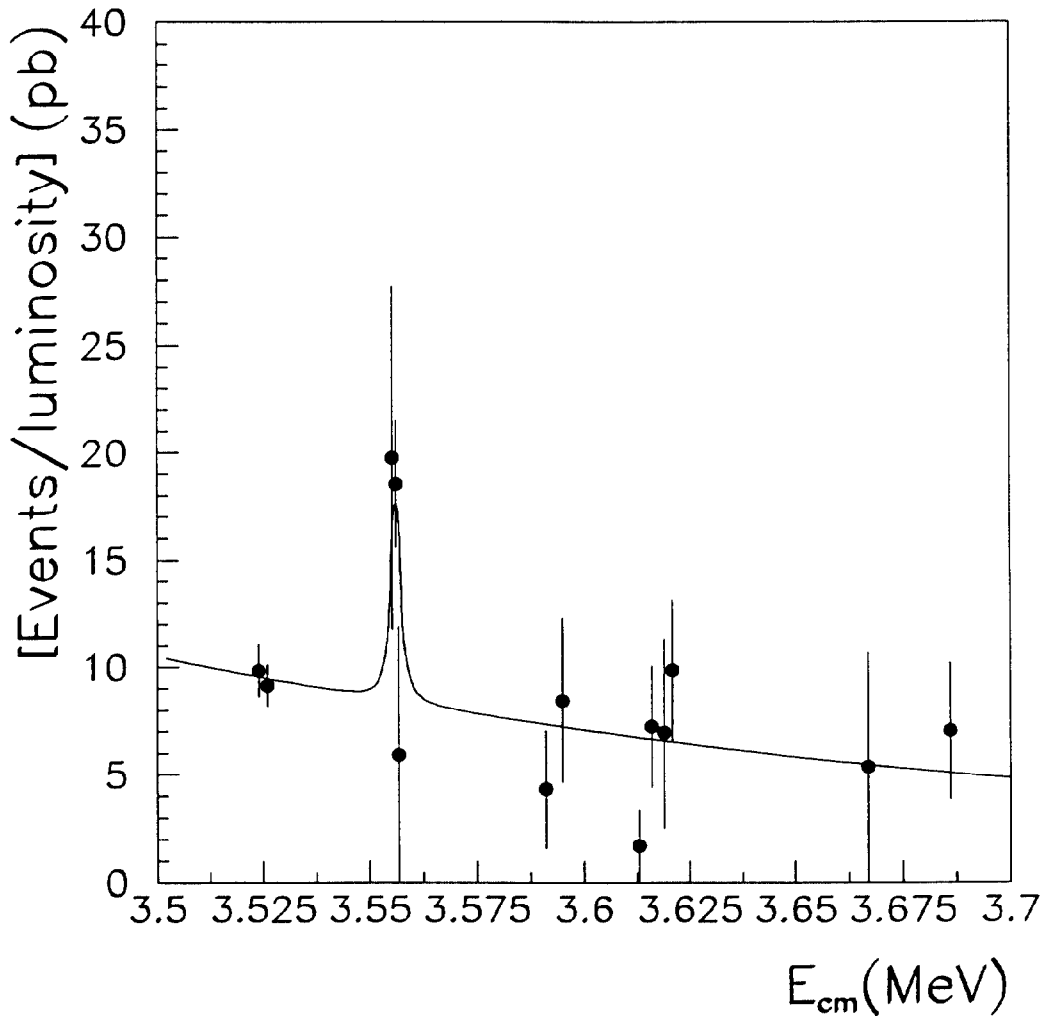


Figure 14 : Measured[50],[39] cross section for  $\bar{p}p \rightarrow \gamma\gamma$  vs center-of-mass energy over an energy range where  $1P$  states, and  $2S$  states are formed. These events were selected cutting at  $|\cos(\theta_\gamma^*)| \leq 0.4$ .

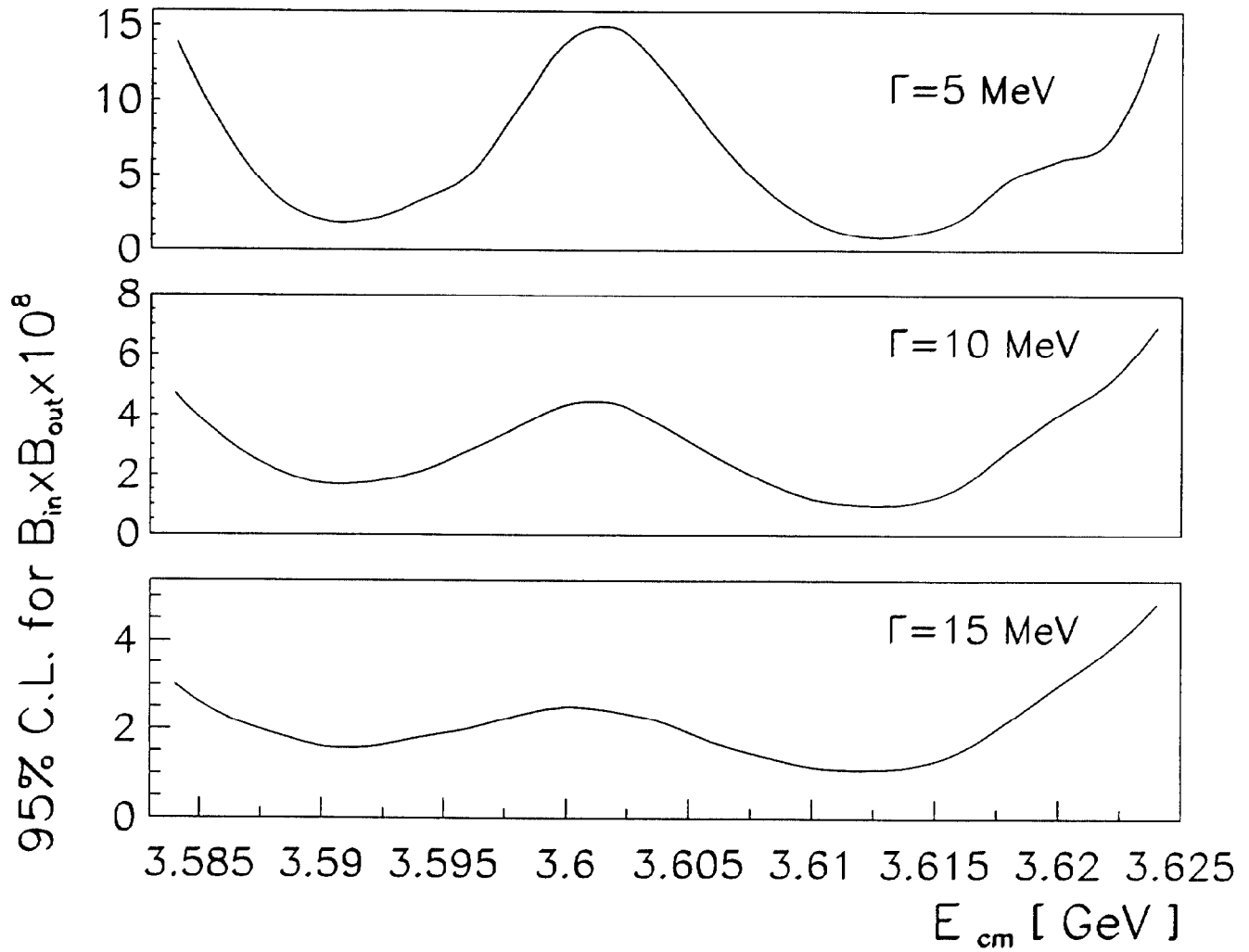


Figure 15 : Search for the  $\eta'_c$  : upper limits[39] on the product  $B_{in} \times B_{out} \times 10^8$ .